

Figure 7. Stimulated embryoid bodies (EBs) adopted the appearance of various types of neuronal cells when injected into spinal cord. (A–C): Almost all the cells derived from stimulated EBs (electropulsed [EP]) displayed MAP2 immunoreactivity, indicating that they had differentiated into mature neurons. Some of the cells derived from EPs expressed ChAT, a motor neuron marker (D–F), or parvalbumin, an inhibitory neuron marker (G–I). Scale bar = 50 μ m.

indicated by expression of several markers including neurotransmitters. Importantly, stimulated EBs showed almost no proliferative activity 50 days after transplantation, unlike ES cells or unstimulated EBs, which showed proliferative and pathogenic features (Fig. 6). Because cells derived from stimulated EBs were extremely efficient in assuming a course of neuronal differentiation in an *in vivo* environment, they hold much promise for use in therapeutic applications.

Ca^{2+} is one of the most important signaling ions involved in various biological activities [19]. Ca^{2+} also appears to play an important role in the system we studied. We found that Ca^{2+} influx was necessary for neural fate determination of EBs. Our finding indicates that this influx did not result from cell membrane fissures; rather, it appears that Ca^{2+} channels may be responsible for Ca^{2+} uptake in our system for the three following reasons: (a) passive influx via membrane fractures results in a much higher magnitude of intracellular fluorescence than what we observed in this study, (b) dye in the culture medium failed to enter the cells upon electrical stimulation, and (c) the original ES cells that did not take on a neuronal fate after electrical stimulation showed no evidence of Ca^{2+} influx (Fig. 3C). We attempted to identify these Ca^{2+} channels by culturing electrically stimulated EBs in media containing agents that block three major Ca^{2+} channels. Treatment with nifedepine, an L-type Ca^{2+} channel blocker, and ω -conotoxins, N- and P/Q-type blockers, failed to block Ca^{2+} influx. Although the existence of these major Ca^{2+} channels in EBs could not be excluded, we conclude that EBs most likely express other minor Ca^{2+} transporters and that these channels mediate the Ca^{2+} influx necessary for neuronal cell fate determination in this system. We conclude that EB formation is required for activation of these Ca^{2+} ion transporters, because, unlike EBs, ES

www.StemCells.com

cells showed no change in intracellular Ca^{2+} density after electrical stimulation.

Ca^{2+} is also known to be involved in the noncanonical *Wnt* signaling pathway. In *Xenopus* and zebrafish, some *Wnt* ligands stimulate release of intracellular Ca^{2+} during development [36]. This Ca^{2+} release, however, induces differentiation into elements (e.g., non-neuronal cells) fated to become ventrally located structures [37]. This is in stark contrast to our system, in which Ca^{2+} induces differentiation into elements (e.g., neuronal cells) fated to become dorsally located structures.

In spite of our efforts, we do not fully understand the mechanisms for this differentiation system. Although we successfully demonstrated that the Ca^{2+} flux is required for the induction (Fig. 3), this will not fully interpret the system. It is possible that other ions, such as potassium or sodium, can also be involved [38]. We are underway to further understand the mechanisms of neuronal induction ability of electrical stimulation on ES cells.

Signaling pathways that transmit information out of cells into the environment are usually activated by receptor-ligand recognition. However, in the present experiments, physical alteration of cell surface membranes may initiate signaling, even though the normal signaling molecule takes over later. This primitive signaling pathway may be a prototype that mediates environmental effects on cells. Receptor-ligand signaling systems may have evolved for stabilization and refinement of environmental cues impinging on cells. This simple system may possibly be invoked during early development and neuronal regeneration. In neuronal tissues, ionic currents are continuously flowing, and these currents may instruct and ensure that undifferentiated cells assume the fate of neuronal progenitors. Ionic flux, therefore, may be a novel category of differentiation signals. Indeed, recent findings show that excitatory neural activity induces adult neural stem cells to adopt a neural fate [39, 40]. In our study, we observed that cells affected by ionic currents were very close to being in an undifferentiated state. The effective differentiation step, therefore, corresponds to states that occur earlier than the neural stem cell state, because unstimulated cells could adopt various cell fates. Even though further studies are required to investigate the physiological role of ionic flow in early embryos, our observations suggest that transmembrane ion flow may play an integral role in early stages of development.

In summary, we described a simple and novel procedure for producing neural cells from ES cells. Further studies are needed to improve our procedure so that parameters are appropriate for therapeutic applications.

ACKNOWLEDGMENTS

We thank A. Nagy, J. Miyazaki, and R. Darnell for the gift of reagents. We also thank S. Itoharu for sharing the ES cell facility, and N. Nakatani for useful discussions. Monoclonal antibodies against *Islet1*, *Pax6*, *Pax7*, *MNR2*, *Nkx2.2*, and *Lim3* developed by T.M. Jessell were obtained from the Developmental Studies Hybridoma Bank under the auspices of NICHD and maintained by University of Iowa. T.K. thanks M. Muramatsu for continuous encouragement, I. Naganuma for secretarial work, and the late G. Matsumoto for help in establishing the laboratory. M.Y. is a recipient of a grant-in-aid for Young Scientists from The Ministry of Education, Culture, Sports, and Technology (MEXT) of Japan. T.K. is supported by a grant from the Human Frontier Scientific Program Orga-

nization and a grant-in-aid for Scientific Research on Priority Areas from MEXT of Japan. All mice were maintained at the animal facilities of RIKEN-BSI according to the Institution's guidelines.

REFERENCES

- 1 Miller-Hance WC, LaCorbiere M, Fuller SJ et al. In vitro chamber specification during embryonic stem cell cardiogenesis. *J Biol Chem* 1993;268:25244–25252.
- 2 Coucouvanis E, Martin GR. BMP signaling plays a role in visceral endoderm differentiation and cavitation in the early mouse embryo. *Development* 1999;126:535–546.
- 3 Gratsch TE, O'Shea KS. Noggin and Chordin have distinct activities in promoting lineage commitment of mouse embryonic stem cells. *Dev Biol* 2002;245:83–94.
- 4 Brustle O, Jones KN, Learish RD et al. Embryonic stem cell-derived glial precursors: A source of myelinating transplants. *Science* 1999;285:754–756.
- 5 Lee SH, Lumelsky N, Studer L et al. Efficient generation of mid brain and hindbrain neurons from mouse embryonic stem cells. *Nat Biotechnol* 2000;18:675–679.
- 6 Lumelsky N, Blondel O, Laeng P et al. Differentiation of embryonic stem cells to insulin-secreting structures similar to pancreatic islets. *Science* 2001;292:1389–1394.
- 7 Zhang S-C, Wering M, Duncan ID et al. In vitro differentiation of transplantable neuronal precursors from human embryonic stem cells. *Nat Biotech* 2001;19:1129–1133.
- 8 Kawasaki H, Mizuseki K, Nishikawa S et al. Induction of midbrain dopaminergic neurons from ES cells by stromal cell-derived inducing activity. *Neuron* 2000;28:31–40.
- 9 Tropepe V, Hitoshi S, Sirard C et al. Direct neural fate specification from embryonic stem cells: A primitive mammalian neural stem cell stage acquired through a default mechanism. *Neuron* 2001;30:65–78.
- 10 Wichterle H, Lieberam I, Porter JA et al. Directed differentiation of embryonic stem cells into motor neurons. *Cell* 2002;110:385–397.
- 11 Ying Q-L, Stavridis M, Griffiths D et al. Conversion of embryonic stem cells into neuroectodermal precursors in adherent monoculture. *Nat Biotechnol* 2003;21:183–186.
- 12 West AE, Chen WG, Dalva MB et al. Calcium regulation of neuronal gene expression. *Proc Natl Acad Sci U S A* 2001;98:11024–11031.
- 13 Zhang LI, Poo MM. Electric activity and development of neuronal circuits. *Nat Neurosci* 2001;4 Suppl:1207–1214.
- 14 Nagai T, Ibata K, Park ES et al. A variant of yellow fluorescent protein with fast and efficient maturation for cell-biological applications. *Nat Biotechnol* 2002;20:87–90.
- 15 Niwa H, Yamamura K, Miyazaki J. Efficient selection for high-expression transfectants with a novel eukaryotic vector. *Gene* 1991;108:193–199.
- 16 Tanemura K, Ogura A, Cheong C et al. Dynamic rearrangement of telomeres during spermatogenesis in mice. *Dev Biol* 2005;281:196–207.
- 17 Sawano A, Hama H, Saito N et al. Multicolor imaging of Ca(2+) and protein kinase C signals using novel epifluorescence microscopy. *Biophys J* 2002;82:1076–1085.
- 18 Okada S, Nakamura M, Mikami Y et al. Blockade of interleukin-6 receptor suppresses reactive astrogliosis and ameliorates functional recovery in experimental spinal cord injury. *J Neurosci Res* 2004;76:265–276.
- 19 Crabtree GR, Olson EN. NFAT signaling: Choreographing the social lives of cells. *Cell* 2002;109:S67–S79.
- 20 Tanabe Y, William C, Jessell TM. Specification of motor neuron identity by MNR2 homeodomain protein. *Cell* 1998;95:67–80.
- 21 Tsuchida T, Ensign M, Morton SB et al. Topographic organization of embryonic motor neurons defined by expression of LIM homeobox genes. *Cell* 1994;79:957–970.
- 22 Beattie MS, Bresnahan JC, Komon J et al. Endogenous repair after spinal cord contusion injuries in the rat. *Exp Neurol* 1997;148:453–463.
- 23 Johansson CB, Momma S, Clarke DL et al. Identification of a neural stem cell in the adult mammalian central nervous system. *Cell* 1999;96:25–34.
- 24 Johansson CB, Lothian C, Molin M et al. Nestin enhancer requirements for expression in normal and injured adult CNS. *J Neurosci Res* 2002;69:784–794.
- 25 Nakamura M, Bregman BS. Difference in neurotrophic factor gene expression profiles between neonate and adult rat spinal cord after injury. *Exp Neurol* 2001;169:407–415.
- 26 Okano H. The stem cell biology of the central nervous system. *J Neurosci Res* 2002;69:698–707.
- 27 Nakamura M, Houghtling RA, MacArthur L et al. Differences in cytokine expression profile between acute and secondary injury in adult rat spinal cord. *Exp Neurol* 2003;184:313–325.
- 28 Okano H, Ogawa Y, Nakamura M et al. Transplantation of neural stem cells into the spinal cord after injury. *Semin Cell Dev Biol* 2003;379:1–8.
- 29 Cohan CS. Frequency-dependent and cell-specific effects of electrical activity on growth cone movements of cultured *Helisoma* neurons. *J Neurobiol* 1990;21:400–413.
- 30 Nakae H. Morphological differentiation of rat pheochromocytoma cells (PC12 cells) by electric stimulation. *Brain Res* 1991;558:348–352.
- 31 Manivannan S, Terakawa S. Rapid sprouting of filopodia in nerve terminals of chromaffin cells, PC12 cells, and dorsal root neurons induced by electrical stimulation. *J Neurosci* 1994;14:5917–5928.
- 32 Aniksztejn L, Demarque M, Morozov Y et al. Recurrent CA1 collateral axons in developing rat hippocampus. *Brain Res* 2001;913:195–200.
- 33 McCaig CD, Rajnicel AM, Song B et al. Has electrical growth cone guidance found its potential? *Trends Neurosci* 2002;25:354–359.
- 34 Kessel M, Gruss P. Homeotic transformations of murine vertebrae and concomitant alteration of *Hox* codes induced by retinoic acid. *Cell* 1991;67:89–104.
- 35 Ogawa Y, Sawamoto K, Miyata T et al. Transplantation of in vitro expanded fetal neural progenitor cells results in neurogenesis and functional recovery after spinal cord contusion injury in adult rats. *J Neurosci Res* 2002;69:925–933.
- 36 Pandur P, Maurus D, Kuhl M. Increasingly complex: New players enter the Wnt signaling network. *BioEssays* 2002;24:881–884.
- 37 Kuhl M, Sheldahl LC, Malbon CC et al. Ca²⁺/Calmodulin-dependent protein kinase II is stimulated by Wnt and Frizzled homologs and promotes ventral cell fates in *Xenopus*. *J Biol Chem* 2000;275:12701–12711.
- 38 Yamada M, Nakanishi K, Ohba S et al. Brain-derived neurotrophic factor promotes the maturation of GABAergic mechanisms in cultures hippocampal neurons. *J Neurosci* 2002;22:7580–7585.
- 39 Deisseroth K, Singla S, Toda H et al. Excitation-neurogenesis coupling in adult neural stem/progenitor cells. *Neuron* 2004;42:535–552.
- 40 Spitzer NC, Root CM, Borodinsky LN. Orchestrating neuronal differentiation: Patterns of Ca²⁺ spikes specify transmitter choice. *Trends Neurosci* 2004;27:415–421.

DISCLOSURES

The authors indicate no potential conflicts of interest.



See www.StemCells.com for supplemental material available online.

Electrical Stimulation Modulates Fate Determination of Differentiating Embryonic Stem Cells

Masahisa Yamada, Kentaro Tanemura, Seiji Okada, Akio Iwanami, Masaya Nakamura, Hideaki Mizuno, Michiru Ozawa, Ritsuko Ohyama-Goto, Naohito Kitamura, Masako Kawano, Kyoko Tan-Takeuchi, Chiho Ohtsuka, Atsushi Miyawaki, Akihiko Takashima, Masaharu Ogawa, Yoshiaki Toyama, Hideyuki Okano and Takashi Kondo

Stem Cells 2007;25;562-570; originally published online Nov 16, 2006;
DOI: 10.1634/stemcells.2006-0011

This information is current as of March 4, 2007

**Updated Information
& Services**

including high-resolution figures, can be found at:
<http://www.StemCells.com/cgi/content/full/25/3/562>

Supplementary Material

Supplementary material can be found at:
<http://www.StemCells.com/cgi/content/full/2006-0011/DC1>

 **AlphaMed Press**

From the Cover: Indispensability of the glutamate transporters GLAST and GLT1 to brain development

Toshiko R. Matsugami, Kentaro Tanemura, Michihiro Mieda, Reiko Nakatomi, Keiko Yamada, Takashi Kondo, Masaharu Ogawa, Kunihiro Obata, Masahiko Watanabe, Tsutomu Hashikawa, and Kohichi Tanaka

PNAS 2006;103;12161-12166; originally published online Jul 31, 2006;
doi:10.1073/pnas.0509144103

This information is current as of March 2007.

Online Information & Services	High-resolution figures, a citation map, links to PubMed and Google Scholar, etc., can be found at: www.pnas.org/cgi/content/full/103/32/12161
Supplementary Material	Supplementary material can be found at: www.pnas.org/cgi/content/full/0509144103/DC1
References	This article cites 44 articles, 19 of which you can access for free at: www.pnas.org/cgi/content/full/103/32/12161#BIBL This article has been cited by other articles: www.pnas.org/cgi/content/full/103/32/12161#otherarticles
E-mail Alerts	Receive free email alerts when new articles cite this article - sign up in the box at the top right corner of the article or click here .
Rights & Permissions	To reproduce this article in part (figures, tables) or in entirety, see: www.pnas.org/misc/rightperm.shtml
Reprints	To order reprints, see: www.pnas.org/misc/reprints.shtml

Notes:

Indispensability of the glutamate transporters GLAST and GLT1 to brain development

Toshiko R. Matsugami^{*†}, Kentaro Tanemura^{*5}, Michihiro Mieda^{*}, Reiko Nakatomi[†], Keiko Yamada[†], Takashi Kondo[‡], Masaharu Ogawa[¶], Kunihiro Obata^{**}, Masahiko Watanabe[¶], Tsutomu Hashikawa^{†,††}, and Kohichi Tanaka^{*††††}

^{*}Laboratory of Molecular Neuroscience, School of Biomedical Science and Medical Research Institute, Tokyo Medical and Dental University, 1-5-45 Yushima, Bunkyo-ku, Tokyo 113-8510, Japan; [†]Laboratory for Neural Architecture, [‡]Brain Development Research Group, [¶]Laboratory for Cell Culture Development, and ^{**}Neuronal Circuit Mechanisms Research Group, RIKEN Brain Science Institute, 2-1 Hirosawa, Wako-shi, Saitama 351-0198, Japan; [¶]Department of Anatomy, Hokkaido University Graduate School of Medicine, Sapporo 060-8638, Japan; and ^{††}Precursory Research for Embryonic Science and Technology, Japan Science and Technology Corporation, 4-1-8 Hon-cho, Kawaguchi, Saitama 332-0012, Japan

Edited by Michael V. L. Bennett, Albert Einstein College of Medicine, Bronx, NY, and approved June 22, 2006 (received for review October 19, 2005)

Previous *in vitro* studies have shown that the neurotransmitter glutamate is important in brain development. Paradoxically, loss-of-function mouse models of glutamatergic signaling that are generated by genetic deletion of glutamate receptors or glutamate release show normal brain assembly. We examined the direct consequences on brain development of extracellular glutamate buildup due to the depletion of the glutamate transporters GLAST and GLT1. GLAST/GLT1 double knockout mice show multiple brain defects, including cortical, hippocampal, and olfactory bulb disorganization with perinatal mortality. Here, we report abnormal formation of the neocortex in GLAST/GLT1 mutants. Several essential aspects of neuronal development, such as stem cell proliferation, radial migration, neuronal differentiation, and survival of SP neurons, were impaired. These results provide direct *in vivo* evidence that GLAST and GLT1 are necessary for brain development through regulation of extracellular glutamate concentration and show that an important mechanism is likely to be maintenance of glutamate-mediated synaptic transmission.

axon/dendrite development | cortex | radial fiber

Neuronal activity is important in the process of refining neural connections in the developing brain (1). Activity, however, may also act to influence earlier developmental events, such as proliferation, migration, differentiation, and survival (2, 3). As key mediators of neuronal activity, neurotransmitters released by neuronal activity are thought to have important signaling roles in shaping the early development of the CNS (3). Previous observations suggest that the major excitatory neurotransmitter, glutamate, provides important communication signals in the developing brain. Indeed, glutamate has been shown to modulate cell proliferation, radial migration, neuronal survival linked to apoptosis, and neuronal differentiation (4–7). In contrast to these observations, most studies in which glutamatergic activity was blocked, whether at the level of ligand or receptor, have demonstrated little, if any, developmental defects (8–14). Thus, according to *in vivo* experiments using loss-of-function models, early glutamate signaling appears to be dispensable. However, because compensatory mechanisms, coupled with a redundancy in glutamate receptor mechanisms, could reduce the severity of a brain phenotype in loss-of-function models, glutamate may still play a role at an early stage of brain development. To investigate this issue, we generated a genetically manipulated animal in which glutamate receptors are overstimulated by genetic deletion of glutamate transporters. Glutamate transporters are essential for the maintenance of low extracellular levels of glutamate (15). The glutamate transporters GLAST, GLT1, and EAAC1 are expressed in the embryonic mouse CNS (16). Previous studies demonstrated that mice lacking GLAST, GLT1, or EAAC1 have seemingly normal brain development (17–19). These results raised the possibility that glutamate transporter subtypes can functionally substitute for one another in CNS development. In the present study, we

inactivated two members of the glutamate transporter family to elucidate roles of the glutamate system in CNS development.

Results

GLAST^{-/-}/GLT1^{-/-} Mutants Have Multiple Brain Defects. Normal development of the CNS was observed in mutant mice lacking GLAST/EAAC1 or EAAC1/GLT1 (data not shown). By contrast, mice lacking GLAST/GLT1 died *in utero* [around embryonic days (E17–18)] and exhibited abnormal brain development after E15 (Fig. 1; see also Figs. 8 and 9, which are published as supporting information on the PNAS web site). The lateral ventricles in GLAST^{-/-}/GLT1^{-/-} mice were dilated relative to those in control mice, and alterations in the structure of the pallial-subpallial boundary were observed in the mutant mice (Fig. 1A–D). The E16 neocortex is laminated, with the following layers: marginal zone, cortical plate (CP), subplate (SP), intermediate zone, and ventricular zone (VZ) (Fig. 1E). In the GLAST^{-/-}/GLT1^{-/-} mutants, the CP border on the intermediate zone was obscured, and the SP could not be identified (Fig. 1F). In addition, cell number in the VZ was decreased in mutant brains (23,558.3 ± 111.6 cells per mm² for WT; 20,216.6 ± 119.7 cells per mm² for the double mutant; *n* = 4; *P* < 0.0001; Fig. 1E and F). Moreover, there were distortions in the organization of the hippocampus and the olfactory bulb of GLAST^{-/-}/GLT1^{-/-} mice (Fig. 8). In the hippocampus, pyramidal neurons were less densely packed. In the olfactory bulb of GLAST^{-/-}/GLT1^{-/-} mice, the mitral cell layer was absent. The present study focused on the cortical malformation of GLAST^{-/-}/GLT1^{-/-} mice.

Expression of GLT1 and GLAST in the Embryonic Brain. GLAST is an astrocytic glutamate transporter in the adult CNS (20). Previous immunocytochemical studies have shown that GLT1 is strongly expressed, primarily by astrocytes, in the adult brain (20). However, we have recently demonstrated that GLT1 is also expressed by some neurons in the hippocampus (21). Because the two transporters show dynamic changes in expression during CNS development (16), we examined cellular elements expressing the two transporters in the embryonic cortex of C57BL mice by immunohistochemistry with subtype-specific antibodies. At

Conflict of interest statement: No conflicts declared.

This paper was submitted directly (Track II) to the PNAS office.

Freely available online through the PNAS open access option.

Abbreviations: En, embryonic day *n*; PCNA, proliferating cell nuclear antigen; MAP2, microtubule-associated protein 2; CT, corticothalamic; TC, thalamocortical; Dil, 1,1'-diiododecyl-3,3',3'-tetramethylindocarbocyanine; AMPA, α -amino-3-hydroxy-5-methyl-4-isoxazolepropionic acid; VZ, ventricular zone; CP, cortical plate; SP, subplate.

⁵Present address: Cellular and Molecular Toxicology Division, National Institute of Health Science, 1-18-1 Kamiyoga, Setagayaku, Tokyo 158-8501, Japan.

^{††}To whom correspondence may be addressed. E-mail: tom@brain.riken.jp or tanaka.aud@mri.tmd.ac.jp.

© 2006 by The National Academy of Sciences of the USA

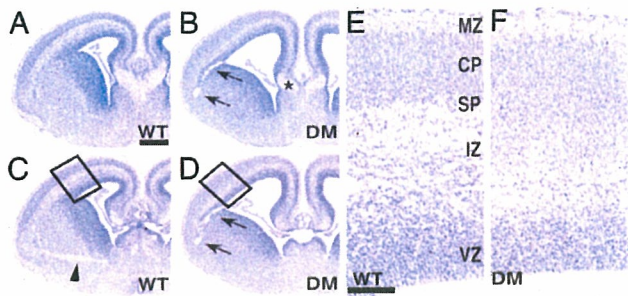


Fig. 1. Morphological abnormalities in brains of $GLAST^{-/-}/GLT1^{-/-}$ mutants. Coronal sections of whole brain (A–D) and neocortex (E and F) at E16 from WT (A, C, and E) and $GLAST^{-/-}/GLT1^{-/-}$ double mutant (DM) (B, D, and F) embryos stained with hematoxylin. Images in A and B are located anterior to those in C and D. Boxed regions in C and D are enlarged in E and F, respectively. The corpus callosum did not cross the midline, and a Probst bundle (asterisk in B) was formed. Arrowhead in C indicates the anterior commissure, which was absent in $GLAST^{-/-}/GLT1^{-/-}$ mutants. Delamination of the pallial–subpallial junction can be seen in the region between arrows in B and D. MZ, marginal zone; IZ, intermediate zone. (Scale bars: A, 500 μm ; E, 100 μm .)

E16, GLT1 was expressed in the globus pallidus, perirhinal cortex, lateral hypothalamus, hippocampus, and fimbria and in the axonal pathways interconnecting the neocortex, basal ganglia, and thalamus (Fig. 2A and C). In the cerebral cortex, GLT1 immunoreactivity was seen in the SP and along fiber bundles in the intermediate zone (Fig. 2C; see also Fig. 10A, which is published as supporting information on the PNAS web site). To investigate further the cellular localization of GLT1 in the cortex, we performed double immunostaining of GLT1 with GAP-43 (growth-associated protein 43), a neuronal marker. GLT1 immunoreactivity was double-labeled by GAP-43, suggesting that GLT1 was expressed in neurons at E16 (Fig. 10). In contrast, GLAST protein was expressed in radial glial cells in the VZ of telencephalon and diencephalon at E16 (Fig. 2B and D). GLAST immunoreactivity was also found in a palisade of radial glial fibers originating in the VZ near the lateral ganglionic eminence–pallium angle and coursing to the pial surface (Fig. 2B). GLT1 and GLAST are thus localized during development on neurons and radial glial cells, respectively, suggesting that the two glutamate transporters might play cooperative and complementary roles in neural development (22). Although GLT1 accounts for $\approx 94\%$ of the total glutamate uptake activity in the adult forebrain (17), both GLAST and GLT1 are major glutamate transporters in the embryonic brain. Therefore, brain development is disturbed in $GLAST/GLT1$ double knockout mice but not in $GLAST$ or $GLT1$ knockout mice.

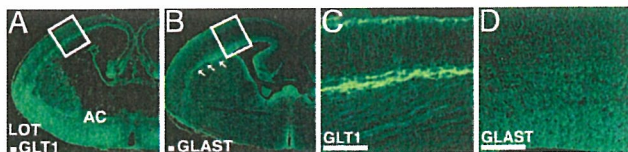


Fig. 2. GLT1 and GLAST immunoreactivity in the mouse forebrain at E16. (A and C) GLT1 was expressed in the globus pallidus, perirhinal cortex, lateral hypothalamus, hippocampus, and fimbria and the axonal pathways interconnecting the neocortex, basal ganglia, and thalamus. (B and D) In contrast, strong GLAST immunoreactivity was seen in radial glial cells and the radial glial fascicle. Boxed regions in A and B are enlarged in C and D, respectively. Arrows in B indicate the radial glial fascicle. AC, anterior commissure; LOT, lateral olfactory tract. (Scale bars: 100 μm .)

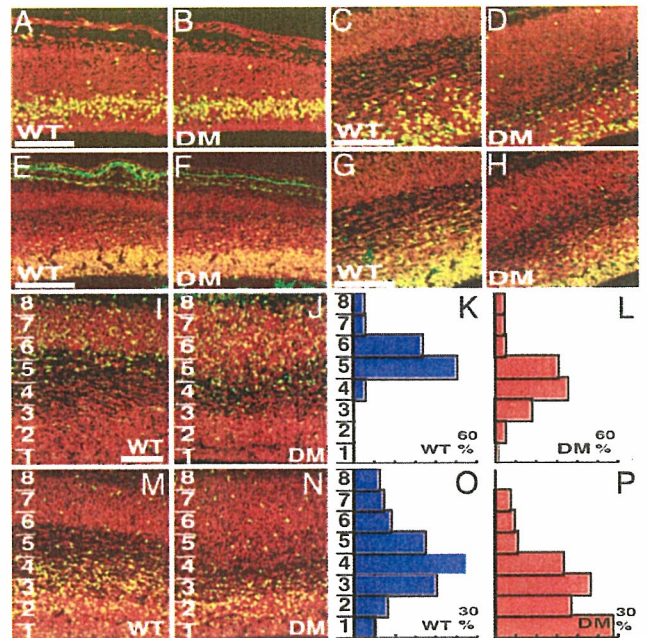


Fig. 3. Reduced cell proliferation and abnormal neural migration in the $GLAST^{-/-}/GLT1^{-/-}$ mutant neocortex. Immunoreactivities of BrdU and PCNA are visualized as green fluorescence. (A–J and M and N) All nuclei were counterstained with propidium iodide (PI) (red). Thus, the BrdU- and PCNA-positive cells appear yellow because they are colabeled for PI and BrdU or PCNA. However, some BrdU- and PCNA-positive cells appear green, because green fluorescence is intensified for easy identification of the BrdU- and PCNA-positive cells. There were a comparable number of BrdU-positive cells in WT (A) and mutant (B) E14 cortices. However, at E16, the number of BrdU-positive cells was reduced in mutant (D) compared with WT (C) cortex. (E–H) PCNA expression at E14 (E and F) and E16 (G and H). BrdU was injected at E12 (I and J) or E14 (M and N), followed by examination of the distribution of BrdU-positive cells at E16. (I–P) To quantify migration, we counted heavily labeled cells (first generation at time of BrdU injection) at E16. The cortices were divided into eight equal areas (numbered 1–8). The percentage of BrdU-positive cells (percentage of total) in each area was determined, and results were plotted as histograms of WT (K and O) and $GLAST^{-/-}/GLT1^{-/-}$ double mutants (DM) (L and P). (Scale bars: 100 μm .)

Cell Birth and Death in the $GLAST^{-/-}/GLT1^{-/-}$ Cortex. A decrease in cell number in the VZ of mutant brains could be caused by reduced cell proliferation or accelerated cell death. To assess the proliferation profile of mutant neuronal progenitors, embryos were pulse-labeled *in utero* with BrdU. At E14, the percentage of BrdU-positive cells in the VZ was similar in WT and mutant mice ($25.0 \pm 1.7\%$ for WT; $26.0 \pm 2.3\%$ for double mutant; $n = 6$; Fig. 3A and B). At E16, however, the percentage of BrdU-positive cells in the VZ was decreased in mutants ($18.3 \pm 0.3\%$ for WT; $16.2 \pm 0.4\%$ for double mutant; $n = 4$; $P < 0.01$; Fig. 3C and D). Proliferation of neuronal progenitor cells was also examined by immunohistochemistry for proliferating cell nuclear antigen (PCNA), a marker of proliferating cells. The pattern of PCNA immunostaining replicated the BrdU results (Fig. 3E–H). This finding is consistent with the results of a previous *in vitro* study that showed that application of glutamate decreased the number of embryonic cortical cells that incorporate BrdU (5). To determine whether cell death was increased in the cortex of double mutants, we used the TUNEL method to stain apoptotic cells. Apoptosis was not increased in the neocortex of mutants at E14 or E16 (data not shown). These results suggest that both GLT1 and GLAST regulate neurogenesis by controlling the extracellular glutamate concentration at E16.

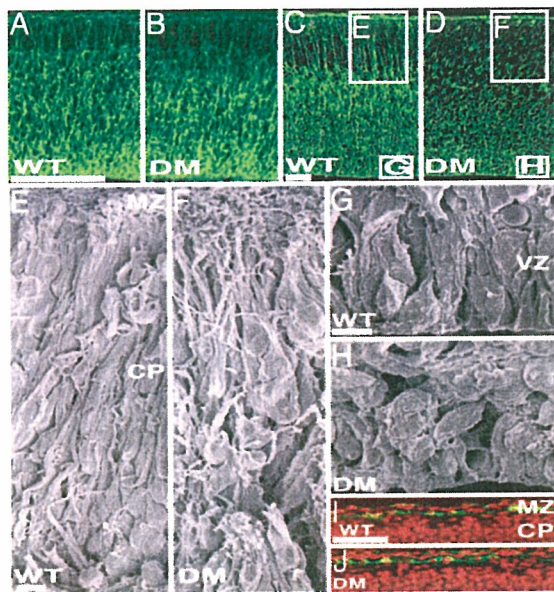


Fig. 4. Altered radial glial systems and normal Reelin expression in $GLAST^{-/-}/GLT1^{-/-}$ mutants. (A–D) Nestin staining of E14 and E16 cortices. The pattern and distribution of radial glial fibers is comparable in WT (A) and double mutant (DM) (B) mice at E14. At E16, however, disruption of radial fibers was apparent in mutant cortices (D) compared with WT (C). (E–H) SEM analysis was performed with E16 cortices. (G) In WT mice, radial glial cells are aligned radially in the VZ. (E) Their radial fibers make bundles and run perpendicular to the pial surface. (F) In $GLAST^{-/-}/GLT1^{-/-}$ mutants, the alignment and density of radial glial fibers are destroyed. (H) In addition, cells in the VZ lost radial morphology. (I and J) In contrast, Reelin expression (green) was comparable in WT (I) and mutant (J) mice at E16. Counterstaining of nuclei was performed with propidium iodide (red). MZ, marginal zone. (Scale bars: A, C, and I, 100 μ m; E and G, 5 μ m.)

Migration of CP Neurons Is Impaired in the $GLAST^{-/-}/GLT1^{-/-}$ Cortex. The disturbed laminar organization of the $GLAST^{-/-}/GLT1^{-/-}$ mutant cortex suggested that cortical cell migrations were abnormal. To investigate neuronal migration *in vivo*, we injected pregnant mice at E12 or E14 with BrdU and examined the labeling patterns at E16. The mutant E12 neurons were spread in a broader gradient compared with WT (Fig. 3 I–L), and the mutant E14 neurons failed to migrate to the CP and remained in the VZ (Fig. 3 M–P). Thus, radial migration is impaired in $GLAST^{-/-}/GLT1^{-/-}$ mutants. Correct neuronal migration requires both the radial glial fibers, which guide postmitotic neurons during their migration, and Cajal–Retzius neurons, which secrete the Reelin protein and thus have a critical role in radial migration. The alignment and density of radial glial fibers stained with anti-nestin antibody were comparable in WT and mutant E14 cortices (Fig. 4 A and B), but the disruption of radial fibers was apparent in mutant E16 cortices (Fig. 4 C and D). SEM analysis also revealed that, at E16, the radial glial fibers in the cerebral wall were disrupted in $GLAST^{-/-}/GLT1^{-/-}$ mutants (Fig. 4 E and F). Furthermore, radial glial cell arrangement was severely disorganized in the VZ of $GLAST^{-/-}/GLT1^{-/-}$ mutants (Fig. 4 G and H). These cells had lost radial morphology but had become round in shape. By contrast, neither the number of Cajal–Retzius neurons nor their immunolabeling intensity for Reelin was changed in the $GLAST^{-/-}/GLT1^{-/-}$ cortex (Fig. 4 I and J). These data suggest that a disrupted radial glial fiber system contributes to the abnormal radial migration of $GLAST^{-/-}/GLT1^{-/-}$ mutants.

Lack of SP Neurons and Defective Cortical Connections in the $GLAST^{-/-}/GLT1^{-/-}$ Mutants. In the double mutants, the SP is difficult to discern (Fig. 1F). Because SP neurons are vulnerable

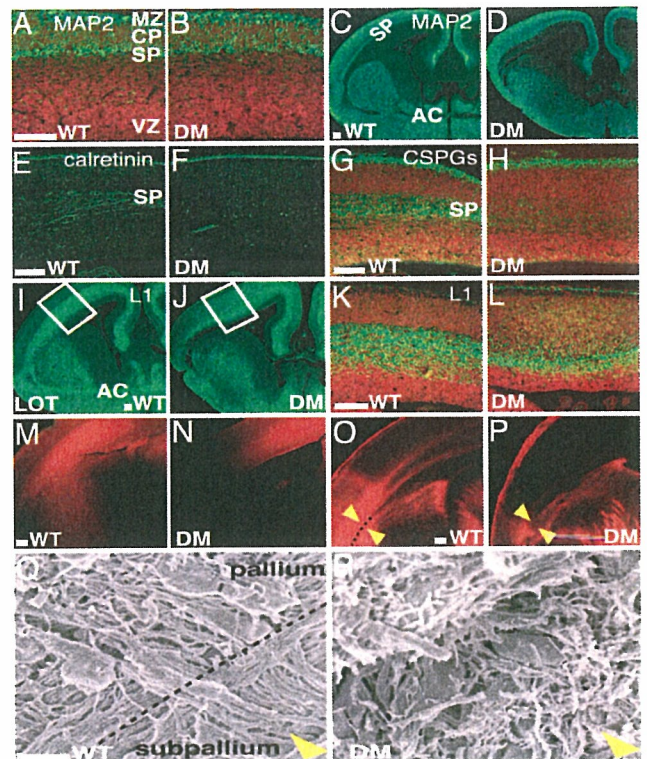


Fig. 5. Loss of SP neurons and impaired cortical connections in $GLAST^{-/-}/GLT1^{-/-}$ mutants. (A–D) MAP2 staining of E14 (A and B) and E16 (C and D) cortices reveals that MAP2-positive SP neurons are difficult to discern in $GLAST^{-/-}/GLT1^{-/-}$ mutants (B and D) at E14 and E16 compared with WT (A and C). (E–H) Immunostaining (green) against calretinin (E and F) and chondroitin sulfate proteoglycans (CSPGs) (G and H) on coronal sections of E16 WT (E and G) and $GLAST^{-/-}/GLT1^{-/-}$ mutant (F and H) cortices shows that SP neurons are mostly missing in mutants. (I–L) Immunostaining (green) against L1 on coronal sections of E16 WT (I and K) and $GLAST^{-/-}/GLT1^{-/-}$ mutant (J and L) cortices reveals defective cortical connections. Boxes in I and J are enlarged in K and L, respectively. All nuclei were stained with propidium iodide (red) in A, B, G, H, K, and L. (M–P) Dil labeling (red) from cortex (M and N) and from thalamus (O and P) at E16 also confirms that TC and CT projections are severely affected in $GLAST^{-/-}/GLT1^{-/-}$ mutants. (M and O) WT. (N and P) $GLAST^{-/-}/GLT1^{-/-}$ mutants. (Q and R) SEM analysis was performed for the region indicated by arrowheads in O and P of E16 WT (Q) and $GLAST^{-/-}/GLT1^{-/-}$ mutant (R) brain. In $GLAST^{-/-}/GLT1^{-/-}$ mutants, the radial glial fascicle at the pallium–subpallium junction is absent, and TC and CT axons cannot cross the junction. DM, double mutant; MZ, marginal zone; AC, anterior commissure; LOT, lateral olfactory tract. (Scale bars: A, C, E, G, I, K, M, and O, 100 μ m; Q, 5 μ m.)

to excitotoxic cell death (23), it is possible that $GLAST^{-/-}/GLT1^{-/-}$ mutants may exhibit SP defects. To investigate possible SP defects in double mutants, we studied microtubule-associated protein 2 (MAP2)-positive SP neurons and expression of SP-specific markers, calretinin and chondroitin sulfate proteoglycans (CSPGs). In double mutants, no MAP2-positive SP neurons were detected at E14 or E16 (Fig. 5 A–D). Furthermore, calretinin and CSPGs were scarcely present in the SP at E16 (Fig. 5 E–H). These results suggest a lack of mature SP neurons in double mutants. SP neurons have been implicated in the development of cortical afferent and efferent connections, including the corticothalamic (CT) and thalamocortical (TC) pathways (23–26). To study these pathways, we used L1 immunostaining and 1,1'-dioctadecyl-3,3,3',3'-tetramethylindocarbocyanine (DiI) tracing. In WT brains, L1-positive fascicles of CT axons pass through the striatum (Fig. 5I). WT L1-positive TC axons leave the diencephalons for the internal capsules and subse-

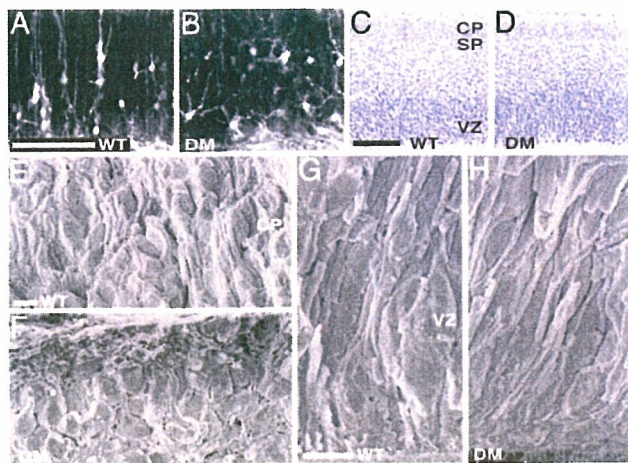


Fig. 6. Impaired maturation of CP neurons in $GLAST^{-/-}/GLT1^{-/-}$ mutants. (A) At E16, pyramidal-like retrogradely labeled cells are observed in the CP of WT mice after DiI injection in the thalamus. (B) In mutants, the morphology and neurite extension of the retrogradely labeled cells were affected. (C and D) Coronal sections of neocortex at E14 from WT mice (C) and $GLAST^{-/-}/GLT1^{-/-}$ mutants (D) stained with hematoxylin. (E–H) SEM analysis was performed with E14 cortices. Although the hematoxylin staining could not reveal impaired maturation of CP neurons in mutants at E14, SEM analysis revealed that the cellular morphology was affected in $GLAST^{-/-}/GLT1^{-/-}$ mutants (F) compared with WT (E). In contrast, the cellular morphology in the VZ was comparable in WT (G) and mutant (H) E14 cortices. DM, double mutants. (Scale bars: A and C, 100 μ m; E and G, 5 μ m.)

quently enter the cortex at E16 (Fig. 5 I and K). In double mutants, L1-positive TC axons scarcely innervated the cortex (Fig. 5 J and L). DiI injection in the cortex at E16 revealed that CT axons did not exit the telencephalon in $GLAST^{-/-}/GLT1^{-/-}$ mutants (Fig. 5 M and N). DiI injection in the thalamus at E16 confirmed that TC axons did not enter the $GLAST^{-/-}/GLT1^{-/-}$ cortex (Fig. 5 O and P). SEM analysis of $GLAST^{-/-}/GLT1^{-/-}$ double mutants revealed that, at E16, the radial glial fascicle at the pallial–subpallial boundary was absent and that CT and TC axons could not cross the pallial–subpallial boundary (Fig. 5 Q and R). The corpus callosum did not cross the midline but formed a Probst bundle (Fig. 1B). Also, the anterior commissure was absent in mutants (Fig. 1D). These results indicate that the TC, CT, and callosal projections are severely affected in $GLAST^{-/-}/GLT1^{-/-}$ mutants.

Maturation of CP Neurons Is Impaired in the $GLAST^{-/-}/GLT1^{-/-}$ Mutants. At E16, pyramidal-like retrogradely labeled cells in the CP after a DiI injection in thalamus were observed in WT mice (Fig. 6A). In contrast, the morphology and neurite outgrowth of the retrogradely labeled cells in the CP were affected in mutant mice (Fig. 6B). To determine the onset of these changes, we examined E14 $GLAST^{-/-}/GLT1^{-/-}$ mutant cortex. Although hematoxylin staining did not show abnormal morphology of CP neurons in the $GLAST^{-/-}/GLT1^{-/-}$ mutants at E14 (Fig. 6C and D), SEM analysis of $GLAST^{-/-}/GLT1^{-/-}$ mutants showed that, at E14, the radial distribution of the CP neurons and their neurites was not conspicuous; these cells had lost their pyramidal-like morphology and had become round in shape (Fig. 6E and F). In contrast, the alignment and density of radial glial cells in the VZ were comparable in WT and mutant E14 cortices (Fig. 6G and H). These results indicate that maturation of CP neurons is impaired in the $GLAST^{-/-}/GLT1^{-/-}$ mutants from E14 onward, whereas abnormal maturation of radial glial cells in the VZ was apparent at E16 (Fig. 4G and H).

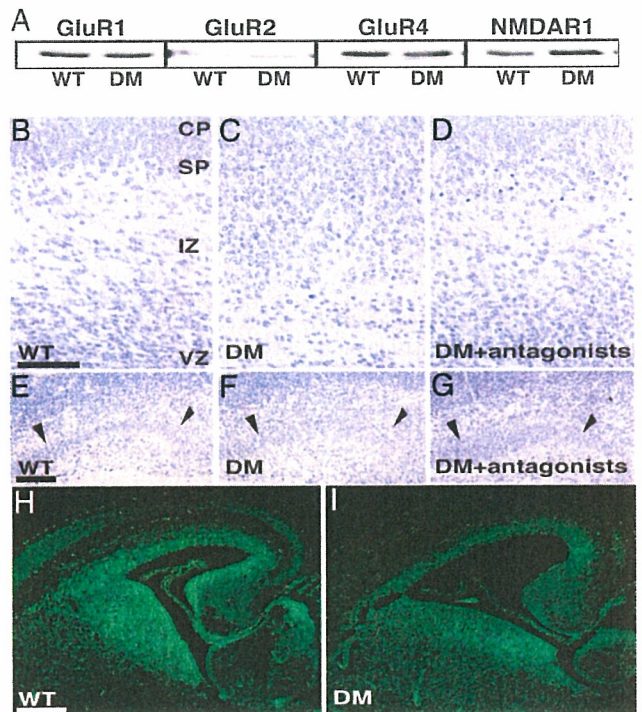


Fig. 7. Partial rescue of the $GLAST^{-/-}/GLT1^{-/-}$ mutant brain phenotype by injection of glutamate receptor antagonists. (A) The relative expression of the glutamate receptors GluR1, GluR2, and GluR4 and NMDA receptor 1 was unchanged in $GLAST^{-/-}/GLT1^{-/-}$ mice compared with WT animals. (B–G) Coronal sections of cortex (B–D) and sagittal sections of hippocampus (E–G) of E16 WT (B and E), $GLAST^{-/-}/GLT1^{-/-}$ (C and F), and $GLAST^{-/-}/GLT1^{-/-}$ mice treated from E8 to E16 with 2,3-dihydroxy-6-nitro-7-sulfamoylbenzo[f]quinoxaline (NBQX) and CGS-19755 (D and G) stained with hematoxylin. Injections of both NBQX and CGS-19755 resulted in a partial rescue of the abnormal stratification of the mutant cerebral cortex and hippocampus. Arrowheads in E–G indicate the pyramidal cell layer in the hippocampus. (H and I) *In situ* hybridization using NARG1 riboprobe on coronal sections of E16 WT (H) and $GLAST^{-/-}/GLT1^{-/-}$ mutants (I). The expression of NARG1 was down-regulated in mutants. DM, double mutants; IZ, intermediate zone. (Scale bar: 100 μ m.)

Partial Rescue of the $GLAST^{-/-}/GLT1^{-/-}$ Brain Phenotypes by Glutamate Receptor Antagonists. Because we previously showed that basal levels of extracellular glutamate in the hippocampus of $GLT1^{-/-}$ mutant mice were significantly higher than those of WT mice (27), it is reasonable to expect that genetic deletion of both $GLT1$ and $GLAST$ would bring about an increase in extracellular glutamate levels, resulting in cortical malformation by excess activation of glutamate receptors. To assess this hypothesis, we first examined whether expression of glutamate receptors is affected in the $GLAST^{-/-}/GLT1^{-/-}$ mutant cortex. The relative expression of the glutamate receptors GluR1, GluR2, and GluR4 and NMDA receptor 1 was unchanged in $GLAST^{-/-}/GLT1^{-/-}$ mice compared with WT animals ($n = 3$ for each) (Fig. 7A). Next, we examined whether the $GLAST^{-/-}/GLT1^{-/-}$ brain phenotype could be reversed by pharmacological administration of glutamate receptor antagonists. Injections of both the α -amino-3-hydroxy-5-methyl-4-isoxazolepropionic acid (AMPA) receptor antagonist 2,3-dihydroxy-6-nitro-7-sulfamoylbenzo[f]quinoxaline (NBQX) and the NMDA receptor antagonist CGS-19755 in pregnant mice between E8 and E16 resulted in a partial rescue of the abnormal stratification of the mutant cerebral cortex (Fig. 7B–D) and hippocampus (Fig. 7E and G). In $GLAST^{-/-}/GLT1^{-/-}$ mutants treated with glutamate receptor antagonists, the cerebral cortex showed some restoration of laminar structure, although it remained

less organized than in WT mice (Fig. 7B–D). The hippocampus of $GLAST^{-/-}/GLT1^{-/-}$ mice is characterized by loose packing of pyramidal neurons (Fig. 7F). In contrast, $GLAST^{-/-}/GLT1^{-/-}$ mice treated with glutamate receptor antagonists had hippocampal formations that seemed almost indistinguishable from WT hippocampus (Fig. 7E and G). The excess activation of the NMDA receptors in $GLAST^{-/-}/GLT1^{-/-}$ mutant brains was also suggested by the examination of expression levels of NMDA receptor-regulated gene 1 (NARG1). A previous study demonstrated that NARG1 is down-regulated by NMDA receptor activation (28). We found that NARG1 mRNA expression was down-regulated in $GLAST^{-/-}/GLT1^{-/-}$ mutant brains by *in situ* hybridization (Fig. 7H and I) and real-time quantitative PCR (Fig. 11, which is published as supporting information on the PNAS web site). Injection of the NMDA receptor antagonist CGS-19755 alone could not rescue the $GLAST^{-/-}/GLT1^{-/-}$ brain phenotypes. Moreover, both the AMPA receptor antagonist and the NMDA receptor antagonist only partially rescued the cortical malformation of mutant mice, suggesting that, in addition to excess activation of both AMPA and NMDA receptors, overactivation of other glutamate receptors, including metabotropic glutamate receptors, may contribute to the multiple severe defects in $GLAST^{-/-}/GLT1^{-/-}$ mutants.

Oxidative Glutamate Toxicity Does Not Contribute to the Cortical Malformation of $GLAST^{-/-}/GLT1^{-/-}$ Mice. Excessive extracellular glutamate leads to cell injury by means of both glutamate receptor-mediated and glutamate receptor-independent mechanisms (29). Glutamate receptor-independent toxicity is caused by oxidative glutamate toxicity. In oxidative glutamate toxicity, high levels of glutamate block the cystine/glutamate exchange system Xc^{-} , resulting in glutathione depletion and cell injury (30). To determine whether oxidative glutamate toxicity is involved in the cortical malformation of $GLAST^{-/-}/GLT1^{-/-}$ mice, we measured the total cortical glutathione levels. Total glutathione levels were slightly increased in the cortex of $GLAST^{-/-}/GLT1^{-/-}$ mice at E16 compared with WT levels (Fig. 12, which is published as supporting information on the PNAS web site), demonstrating that oxidative glutamate toxicity does not play a significant role in the cortical malformation of $GLAST^{-/-}/GLT1^{-/-}$ mice.

Discussion

A large body of *in vitro* evidence indicates that the neurotransmitter glutamate acts to influence earlier developmental events, such as proliferation, migration, and differentiation (4–7). However, nearly all of the genetic experiments to date, in which glutamatergic signaling was blocked, have shown little, if any, developmental defects (8–14). Our work represents a unique analysis of the direct consequences on brain development of extracellular glutamate buildup due to the depletion of glutamate transporters. In contrast to loss-of-function studies, *in vivo* excess activation of glutamate receptors can modulate brain maturation, such as stem cell proliferation, radial migration, survival of SP neurons, and neuronal differentiation, including neurite elongation and path finding. This discrepancy may be due to compensation by other neurotransmitters such as GABA, acetylcholine (ACh), and glycine, all of which can depolarize embryonic cortical neurons as does glutamate (31). GABA is also one of the most abundant neurotransmitters detected during mammalian brain development, and its involvement in shaping brain development has also been suggested by recent *in vitro* investigations (5, 32, 33). However, mice lacking the two primary GABA biosynthetic enzymes, GAD65 and GAD67, show no discernible defects of neural development despite having only 0.02% of the normal GABA content (34). This discrepancy might also be due to compensation by other neurotransmitters *in vivo*. Glutamate, GABA, ACh, and glycine can all depolarize embryonic cortical neurons, so pathways involving more than

one of these transmitters could potentially show mitigated severity of defects in single-neurotransmitter loss-of-function mutations. In the future, it will be important to analyze the direct consequences of overactivation of individual neurotransmitter receptors. Such studies could reveal functional roles of early appearing transmitter signaling during development.

The prevailing view of CNS development is that neural activity is, for the most part, important only in the refinement of axonal projections and synaptic connections, whereas early development of the nervous system is likely to be genetically programmed. Two recent studies have challenged this view by providing evidence that neural activity is required for spinal motor neurons to make accurate early path-finding decisions (35) and for embryonic spinal cord neurons to determine which types of neurotransmitters to produce (36). Combined with these studies, the present study suggests that neural activity is likely to be important in shaping early brain development and that glutamate, as a key mediator of neural activity, may play an important role in shaping the early CNS development. For these influences to be physiologically relevant, however, glutamate must be released at an early developmental stage and diffuse to stimulate glutamate receptors. Several observations support this hypothesis: (i) functional glutamate receptors are expressed by neuronal precursors and neurons of several brain areas at a very early stage (3, 37), (ii) exocytosis of glutamate occurs from growing axons and cones before synapse formation (38), (iii) paracrine nonvesicular release of glutamate exists before synapse formation and modulates neuronal migration (39, 40), and (iv) an efficient glutamate transport system is operative at early developmental stages (39). Depending on the neural activity and the location and properties of glutamate receptors and transporters, it is possible that excess activation of glutamate receptors can occur and modulate brain development. Therefore, normal brain development requires tight control of extracellular glutamate by the glutamate transporters $GLAST$ and $GLT1$. This hypothesis was also confirmed by the severe developmental defects that were observed in the regions of the brain where both $GLAST$ and $GLT1$ are expressed, such as the inner half of the cortex, the pallidum–subpallidum boundary, and the SP neurons (Fig. 13, which is published as supporting information on the PNAS web site). $GLAST^{-/-}/GLT1^{-/-}$ double mutants have enabled us to clarify how glutamatergic signaling regulates the molecular pathways that control brain development.

Previous *in vitro* studies demonstrated that glutamate is involved in modulating the radial migration of cortical projection neurons. Blockade of NMDA receptors decreases cell migration, whereas enhancement of NMDA receptor activity or inhibition of extracellular glutamate uptake increases the rate of cell movement (4, 7). Interestingly, radial migration is impaired in $GLAST^{-/-}/GLT1^{-/-}$ double mutants, in which excess activation of the NMDA receptor may occur. This impairment could be attributed to the fact that excess activation of glutamate receptors in $GLAST^{-/-}/GLT1^{-/-}$ double mutants leads to disruption of the radial glial fiber system. Recent studies have indicated that glutamate released from corticofugal axons could lead to NMDA and AMPA/kainate receptor activation in tangentially migrating cells and thereby modulate their response to guidance cues (41, 42). Furthermore, $GLT1$ is expressed in corticofugal axons. Future experiments investigating the tangential migration of interneurons in $GLAST^{-/-}/GLT1^{-/-}$ double mutants may clarify the functional significance of glutamate for tangential migration as well as radial migration.

It has been shown that SP cells are necessary for the development of many efferent and afferent cortical connections (23–26). We found that SP neurons were deficient in the neocortex of $GLAST^{-/-}/GLT1^{-/-}$ mutants from E14 onward. Consistent with the defect in SP neurons, TC and CT projections were lacking in mutant mice.

Abnormal development of the brain during fetal life is now thought to contribute to the etiology of many neurological disorders that manifest throughout life (43). Cerebral hypoxia-ischemia is considered to be a major cause of perinatal brain injury. A dysfunction of glutamate transporters and the resulting excess glutamate are important pathophysiological mechanisms in brain injury after hypoxia-ischemia. Therefore, GLAST^{-/-}/GLT1^{-/-} mutants may be useful for characterizing lesions formed in response to hypoxia-ischemia and for developing neuroprotective strategies to reduce the burden of altered brain growth and poor functional and behavioral outcomes (44).

Materials and Methods

Mice. The GLT1, GLAST, and EAAC1 mutant mice are described in refs. 17–19. To generate all combinations of double mutants, double-heterozygous mice (GLT1^{+/-}/GLAST^{+/-}, GLAST^{+/-}/EAAC1^{+/-}, and EAAC1^{+/-}/GLT1^{+/-}) were crossed. All mice were on a C57BL/6J background. The day of vaginal plug detection was designated as E0.5.

- Cohen-Cory, S. (2002) *Science* **298**, 770–776.
- Ben-Ari, Y. (2001) *Trends Neurosci.* **24**, 353–360.
- Nguyen, L., Rigo, J. M., Rocher, V., Belachew, S., Malgrange, B., Rogister, B., Leprince, P. & Moonen, G. (2001) *Cell Tissue Res.* **305**, 187–202.
- Komuro, H. & Rakic, P. (1993) *Science* **260**, 95–97.
- LoTurco, J. J., Owens, D. F., Heath, M. J., Davis, M. B. & Kriegstein, A. R. (1995) *Neuron* **15**, 1287–1298.
- Ikonomidou, C., Bosch, F., Miksa, M., Bittigau, P., Vockler, J., Dikranian, K., Tenkova, T. I., Stefovská, V., Turski, L. & Olney, J. W. (1999) *Science* **283**, 70–74.
- Behar, T. N., Scott, C. A., Greene, C. L., Wen, X., Smith, S. V., Maric, D., Liu, Q. Y., Colton, C. A. & Barker, J. L. (1999) *J. Neurosci.* **19**, 4449–4461.
- Kutsuwada, T., Sakimura, K., Manabe, T., Takayama, C., Katakura, N., Kushiya, E., Natsume, R., Watanabe, M., Inoue, Y., Yagi, T., et al. (1996) *Neuron* **16**, 333–344.
- Messersmith, E. K., Feller, M. B., Zhang, H. & Shatz, C. J. (1997) *Mol. Cell Neurosci.* **9**, 347–357.
- Zamanillo, D., Sprengel, R., Hvalby, O., Jensen, V., Burnashev, N., Rozov, A., Kaiser, K. M., Koster, H. J., Borchardt, T., Worley, P., et al. (1999) *Science* **284**, 1805–1811.
- Meng, Y., Zhang, Y. & Jia, Z. (2003) *Neuron* **39**, 163–176.
- Verhage, M., Maia, A. S., Plomp, J. J., Brussaard, A. B., Heeroma, J. H., Vermeer, H., Toonen, R. F., Hammer, R. E., van den Berg, T. K., Missler, M., et al. (2000) *Science* **287**, 864–869.
- Wojcik, S. M., Rhee, J. S., Herzog, E., Sigler, A., Jahn, R., Takamori, S., Brose, N. & Rosenmund, C. (2004) *Proc. Natl. Acad. Sci. USA* **101**, 7158–7163.
- Fremcau, R. T., Jr., Kam, K., Qureshi, T., Johnson, J., Copenhagen, D. R., Storm-Mathisen, J., Chaudhry, F. A., Nicoll, R. A. & Edwards, R. H. (2004) *Science* **304**, 1815–1819.
- Tanaka, K. (2000) *Neurosci. Res.* **37**, 15–19.
- Shibata, T., Watanabe, M., Tanaka, K., Wada, K. & Inoue, Y. (1996) *NeuroReport* **7**, 705–709.
- Tanaka, K., Watase, K., Manabe, T., Yamada, K., Watanabe, M., Takahashi, K., Iwama, H., Nishikawa, T., Ichihara, N., Kikuchi, T., et al. (1997) *Science* **276**, 1699–1702.
- Peghini, P., Janzen, J. & Stoffel, W. (1997) *EMBO J.* **16**, 3822–3832.
- Watase, K., Hashimoto, K., Kano, M., Yamada, K., Watanabe, M., Inoue, Y., Okuyama, S., Sakagawa, T., Ogawa, S., Kawashima, N., et al. (1998) *Eur. J. Neurosci.* **10**, 976–988.
- Danbolt, N. C. (2001) *Prog. Neurobiol.* **65**, 1–105.
- Chen, W., Mahadomrongkul, V., Berger, U. A., Bassan, M., DeSilva, T., Tanaka, K., Irwin, N., Aoki, C. & Rosenberg, P. A. (2004) *J. Neurosci.* **24**, 1136–1148.
- Yamada, K., Watanabe, M., Shibata, T., Nagashima, M., Tanaka, K. & Inoue, Y. (1998) *J. Neurosci.* **18**, 5706–5713.
- McConnell, S. K., Ghosh, A. & Shatz, C. J. (1994) *Neuroscience* **14**, 1892–1907.
- Hevner, R. F., Shi, L., Justice, N., Hsueh, Y., Sheng, M., Smiga, S., Bulfone, A., Goffinet, A. M., Campagnoni, A. T. & Rubenstein, J. L. (2001) *Neuron* **29**, 353–366.
- Ghosh, A., Antonini, A., McConnell, S. K. & Shatz, C. J. (1990) *Nature* **347**, 179–181.
- De Carlos, J. A. & O'Leary, D. D. (1992) *J. Neurosci.* **12**, 1194–1211.
- Mitani, A. & Tanaka, K. (2003) *J. Neurosci.* **23**, 7176–7182.
- Sugiura, N., Patel, R. G. & Corriveau, R. A. (2001) *J. Biol. Chem.* **276**, 14257–14263.
- Schubert, D. & Piasecki, D. (2001) *J. Neurosci.* **21**, 7455–7462.
- Rimaniol, A. C., Mialocq, P., Clayette, P., Dormont, D. & Gras, G. (2001) *Am. J. Physiol.* **281**, C1964–C1970.
- Ben-Ari, Y. (2002) *Nat. Rev. Neurosci.* **3**, 728–739.
- Behar, T. N., Li, Y. X., Tran, H. T., Ma, W., Dunlap, V., Scott, C. & Barker, J. L. (1996) *J. Neurosci.* **16**, 1808–1818.
- Obata, K. (1997) *Dev. Neurosci.* **19**, 117–119.
- Ji, F., Kanbara, N. & Obata, K. (1999) *Neurosci. Res.* **33**, 187–194.
- Hanson, M. G. & Landmesser, L. T. (2004) *Neuron* **43**, 687–701.
- Borodinsky, L. N., Root, C. M., Cronin, J. A., Sann, S. B., Gu, X. & Spitzer, N. C. (2004) *Nature* **429**, 523–530.
- Lujan, R., Shigemoto, R. & Lopez-Bendito, G. (2005) *Neuroscience* **130**, 567–580.
- Soeda, H., Tatsumi, H. & Katayama, Y. (1997) *Neuroscience* **77**, 1187–1189.
- Demarque, M., Repra, A., Becq, H., Khalilov, I., Ben-Ari, Y. & Anirsztejn, L. (2002) *Neuron* **36**, 1051–1061.
- Manent, J. B., Demarque, M., Jorquera, I., Pellegrino, C., Ben-Ari, Y., Anirsztejn, L. & Repra, A. (2005) *J. Neurosci.* **25**, 4755–4765.
- Poluch, S., Drian, M. J., Durand, M., Astier, C., Benyamin, Y. & Konig, N. (2001) *J. Neurosci. Res.* **63**, 35–44.
- Soria, J. M. & Valdeolmillos, M. (2002) *Cereb. Cortex* **12**, 831–839.
- Rees, S. & Inder, T. (2005) *Early Hum. Dev.* **81**, 753–761.
- Tanaka, K. (2005) *Trends Mol. Med.* **11**, 259–262.
- Simonian, S. X. & Herbison, A. E. (2001) *J. Neurosci.* **21**, 934–943.

Histological Analysis, BrdU Labeling, TUNEL Assay, Western Blot Analysis, Real-Time PCR, and Glutathione Assay. All detailed information specific to the experiments described here can be found in *Supporting Materials and Methods*, which is published as supporting information on the PNAS web site.

Effect of AMPA and NMDA Receptor Antagonism on Brain Abnormalities of Mutant Mice. This experiment was performed as described in ref. 45. Between E8 and E16, pregnant mice received i.p. injections of the AMPA and NMDA receptor antagonists. Detailed procedures are described in *Supporting Materials and Methods*.

We thank R. A. Corriveau (Wayne State University, Detroit, MI) for his gift of the NARG1 probe and H. Kamiguchi (RIKEN Brain Science Institute) for his gift of the L1 antibody. This work was supported by research grants from RIKEN Brain Science Institute; a grant-in-aid for Scientific Research from the Japan Society for the Promotion of Sciences; and a grant-in-aid for Scientific Research on Priority Areas from the Ministry of Education, Culture, Sports, and Technology of Japan (to K. Tanaka).

Formation of Tau Inclusions in Knock-in Mice with Familial Alzheimer Disease (FAD) Mutation of Presenilin 1 (PS1)*

Received for publication, August 19, 2005, and in revised form, December 21, 2005. Published, JBC Papers in Press, December 23, 2005, DOI 10.1074/jbc.M509145200

Kentaro Tanemura[†], Du-Hua Chui^{†1}, Tetsuya Fukuda[†], Miyuki Murayama[†], Jung-Mi Park[†], Takumi Akagi[§], Yoshitaka Tatebayashi[†], Tomohiro Miyasaka[†], Tetsuya Kimura[†], Tsutomu Hashikawa[§], Yuka Nakano[¶], Takashi Kudo[¶], Masatoshi Takeda[¶], and Akihiko Takashima^{†2}

From the [†]Laboratory for Alzheimer Disease and [§]Neural Architecture, Brain Science Institute, RIKEN, Wako, Saitama 351-0198, Japan and the [¶]Department of Psychiatry and Behavioral Science and Environmental Medicine, Osaka University Graduate School of Medicine, 2-2 Yamadaoka, Suita, Osaka 565-0871, Japan

Mutations in the presenilin 1 (*PS1*) gene are responsible for the early onset of familial Alzheimer disease (FAD). Accumulating evidence shows that PS1 is involved in γ -secretase activity and that FAD-associated mutations of PS1 commonly accelerate $A\beta_{1-42}$ production, which causes Alzheimer disease (AD). Recent studies suggest, however, that PS1 is involved not only in $A\beta$ production but also in other processes that lead to neurodegeneration. To better understand the causes of neurodegeneration linked to the PS1 mutation, we analyzed the development of tau pathology, another key feature of AD, in PS1 knock-in mice. Hippocampal samples taken from FAD mutant (I213T) PS1 knock-in mice contained hyperphosphorylated tau that reacted with various phosphodependent tau antibodies and with Alz50, which recognizes the conformational change of PHF tau. Some neurons exhibited Congo red birefringence and Thioflavin T reactivity, both of which are histological criteria for neurofibrillary tangles (NFTs). Biochemical analysis of the samples revealed SDS-insoluble tau, which under electron microscopy examination, resembled tau fibrils. These results indicate that our mutant PS1 knock-in mice exhibited NFT-like tau pathology in the absence of $A\beta$ deposition, suggesting that PS1 mutations contribute to the onset of AD not only by enhancing $A\beta_{1-42}$ production but by also accelerating the formation and accumulation of filamentous tau.

Alzheimer disease (AD)³ is characterized pathologically by neurofibrillary tangles (NFTs), which are composed of highly phosphorylated tau, and by neuronal loss and $A\beta$ deposition. AD is manifested symptomatically by dementia. Presenilin 1 (*PS1*), a gene identified to be responsible, in part, for early onset familial Alzheimer disease (FAD), has been cloned (1, 2). To date more than 70 mutations of the *PS1* gene have been reported (3, 4). In each mutation, early onset of AD develops with 100% penetration (3, 4). PS1 is required for γ -secretase to cleave amyloid precursor protein into $A\beta$ species such as $A\beta_{1-40}$ and $A\beta_{1-42}$.

Improper cleavage of amyloid precursor protein because of a PS1 mutation increases the production of $A\beta_{1-42}$ (5–7), a highly aggregative, neurotoxic species of $A\beta$ that is longer than the less toxic $A\beta_{1-40}$. One hypothesis for the neurodegeneration observed in AD, therefore, is that PS1 mutation leads to increasing amounts of extracellular, neurotoxic $A\beta_{1-42}$, thereby inducing neurodegeneration (8–11).

Accumulating data suggest that, in addition to its role in $A\beta_{1-42}$ production, PS1 mutation also contributes to NFT formation. For example, PS1 conditional knock-out mice display phosphorylated tau, synaptic dysfunction, and memory impairment, even in the absence of $A\beta$ production and deposition (12). In a related line of research, some patients clinically diagnosed with fronto-temporal dementia (FTD) have been shown to harbor PS1 mutations (13–16). Interestingly, FTD is characterized by the appearance of NFTs without $A\beta$ deposition (17). A patient harboring the G183V PS1 mutation displayed the clinical manifestations of FTD and exhibited phospho-tau-positive Pick body pathology throughout the cortex and limbic region, without $A\beta$ deposition. Other reports have also shown that PS1 mutations accelerate NFT formation and neuronal loss without affecting the rate of $A\beta$ deposition (18). Thus, these data lead to the hypothesis that PS1 mutations might contribute to NFT formation as well as increase $A\beta_{1-42}$ production in FAD.

To investigate this hypothesis, we examined tau pathology in mutant PS1 I213T knock-in mice (19). This line of mice was generated with a targeted insertion of the I213T missense mutation into exon 7 of the mouse *PS1* gene using homologous recombination. Therefore, these PS1 mutant knock-in mice harbor the FAD mutation in the mouse *PS1* gene and produce PS1 I213T. Heterozygote mutant PS1 I213T mice showed no change in $A\beta_{1-40}$ levels but had increased levels of $A\beta_{1-42}$, a 1.3-fold increase when compared with wild-type mice. This $A\beta_{1-42}$ increase is comparable to that observed in human cases. Because this mouse strain shares the same PS1 genotype and related pathology as that of patients harboring the PS1 mutation, we initially expected these mice to develop the AD phenotype. The increase in murine $A\beta_{1-42}$, however, failed to lead to a corresponding $A\beta$ deposition, possibly because murine $A\beta$ has a different amino acid sequence that reduces its tendency to aggregate. Using this dissociation to our advantage, we investigated the $A\beta$ deposition-independent effects of the PS1 mutation in this mouse model. We found that GSK-3 β activation was followed by the accumulation of hyperphosphorylated tau in the hippocampal region, which fulfills the histological criteria for the presence of NFTs.

EXPERIMENTAL PROCEDURES

Animals—Mutant PS1 I213T knock-in mice (mPS1 mice) were maintained at the RIKEN BSI animal facilities according to the Institute guidelines for the treatment of experimental animals.

* This work was supported in part by a grant from the Ministry of Education, Science, Sports, and Culture of Japan. The costs of publication of this article were defrayed in part by the payment of page charges. This article must therefore be hereby marked "advertisement" in accordance with 18 U.S.C. Section 1734 solely to indicate this fact.

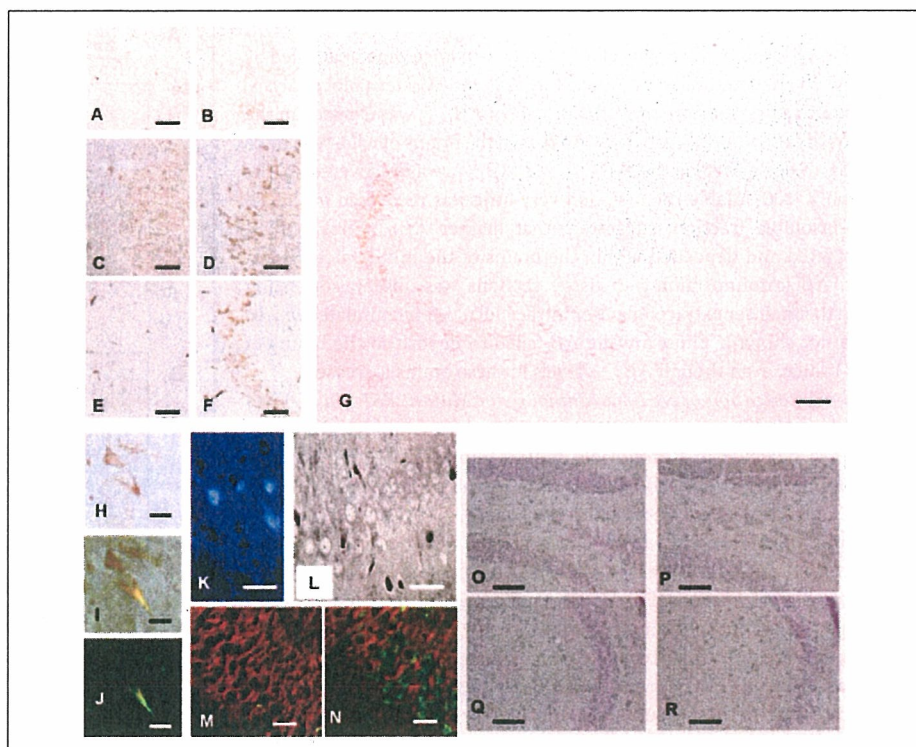
¹ Present address: Neuroscience Research Institute, Peking University, 38 Xue Yuan Rd., Beijing 100083, China.

² To whom correspondence should be addressed: Laboratory for Alzheimer Disease, RIKEN Brain Science Institute, 2-1 Hirosawa, Wako-shi, Saitama 351-0198, Japan. Tel.: 81-48-467-9632; Fax: 81-48-467-5916; E-mail: kenneth@brain.riken.jp.

³ The abbreviations used are: AD, Alzheimer disease; PS1, presenilin 1; FAD, familial Alzheimer disease; $A\beta$, amyloid β protein; NFT, neurofibrillary tangles; FTD, fronto-temporal dementia; GSK-3 β , glycogen synthase kinase-3 β ; PHFs, paired helical filaments; TBS, Tris-buffered saline; CDK5, cyclin-dependent kinase 5; JNK, c-Jun N-terminal kinase; MAP, mitogen-activated protein; TUNEL, terminal deoxynucleotidyltransferase-mediated dUTP nick end-labeling; RIPA, radioimmune precipitation assay buffer.

Tau Inclusions in FAD Mutant PS1 Knock-in Mice

FIGURE 1. Histochemical and histopathological assessment of brain sections from wild-type (wPS1) and mutant PS1 knock-in (mPS1) mice. A–G, anti-tau immunoreactivity in hippocampal CA3 of wPS1 mice (A, C, E) and heterozygous mPS1 mice (B, D, F) at 7 months (A, B) and 15 months (C–G) of age. A–D, PS199 immunoreactivity; E–G, Alz50 immunoreactivity. The low power micrograph in G shows how hippocampal immunoreactivity is confined largely to CA3. H–L, histopathology in CA3 of heterozygous mPS1 mice at 15 months of age. H–J, Congo red staining without (H) or with (I, J) polarizing filters; K, Thioflavin T; and L, Gallyas silver-staining. M and N, immunoreactivity in CA3 of wPS1 (M) and heterozygous mPS1 mice (N) at 16 months of age. M and N, double immunolabeling with α -tubulin (red) and PS199 (green) antibodies. O, TUNEL staining of dentate gyrus in the wPS1 mouse; P, TUNEL staining of dentate gyrus in the homozygous mPS1 mouse; Q, TUNEL staining of CA3 in the wPS1 mouse; R, TUNEL staining of CA3 in the homozygous mPS1 mouse. Scale bars: 50 μ m in A–F and O–R; 100 μ m in G; 10 μ m in H–L; 25 μ m in M and N.



Antibodies—The following antibodies were used: mouse monoclonal anti-tubulin (DM1A, Sigma); anti-ubiquitin (Santa Cruz Biotechnology); anti-GSK3 β (Transduction Laboratory); anti-MAP2 (HM2, Sigma); anti-tau Alz50, which recognizes the conformational epitope of paired helical filaments (PHFs), component of NFT (a generous gift from Dr. P. Davies, Albert Einstein College of Medicine, Bronx, NY); anti-phosphorylated tau AT8 (Innogenetics Zwijndrecht); anti-dephosphorylated tau, Tau-1 (Chemicon); rabbit polyclonal anti-tau JM (20); anti-phosphorylated tau PS199, PS262, PS396, PS404, and PS422 (BIO-SOURCE), which recognize tau phosphorylated at the indicated sites; and anti-GSK3 β Ser-9 (Cell Signaling).

Western Blot Analysis—Brains were homogenized in modified radioimmunoprecipitation assay (RIPA) buffer (50 mM Tris, 150 mM NaCl, 1% Nonidet P-40, 5 mM EDTA, 0.5% sodium deoxycholate, and 0.1% SDS, pH 8.0), and the suspension was centrifuged at 100,000 \times g for 20 min at 4 $^{\circ}$ C in an Optima TL ultracentrifuge (Beckman). The pellet was washed five times with 1% SDS-Tris-buffered saline (TBS) (50 mM Tris, 150 mM NaCl, and 1% SDS, pH 8.0) followed each time by centrifugation. The SDS-insoluble pellet was solubilized in 70% formic acid, lyophilized, reconstituted in Laemmli SDS-PAGE sample buffer, and subjected to SDS-PAGE. Separated proteins were blotted onto Immobilon-P membranes (Millipore). The membranes were incubated with primary antibody then with the species-appropriate horseradish peroxidase-conjugated secondary antibody. Immunoreactivity was visualized with a chemiluminescent detection system (ECL, Amersham Biosciences). Quantitation and visual analysis of immunoreactivity were performed with a computer-linked LAS-1000 Bio-Imaging Analyzer System (Fujifilm) using the software program Image Gauge 3.0 (Fujifilm).

Glycogen Synthase Kinase (GSK)-3 β Activity—Brains were homogenized in TBS (pH 7.4) and centrifuged at 100,000 \times g for 20 min at 4 $^{\circ}$ C in an Optima TL ultracentrifuge (Beckman). Protein concentration in

the supernatant was determined with a Bradford protein assay, and 10- μ g samples were assayed for GSK-3 β activity with an immunoprecipitation assay (21).

Ultrastructural Studies—For electron microscopy studies, SDS-insoluble materials were prepared from the brains of mPS1 mice as described above in the Western blot analysis section. The materials were mildly sonicated and dispersed in phosphate-buffered saline. The dispersed solution was absorbed onto glow-discharged supporting membranes on 400-mesh grids and prefixed by floating the grids on drops of 4% paraformaldehyde in 0.1 M phosphate buffer for 5 min. After washing, the grids were incubated with primary antibody (JM, anti-tau antibody), followed with a 5-nm colloidal gold-conjugated secondary antibody. The grids were then negatively stained with 2% sodium phosphotungstic acid, dried, and observed with a LEO 912AB electron microscope at 100 kV.

Immunohistochemical and Histopathological Studies—Brains were immersion-fixed in 10%-buffered formalin, and paraffin-embedded sections (4 μ m) were prepared. PS199, Alz50, anti-MAP2, and AT8 were used as primary antibodies. After reacting the sections with species-appropriate secondary antibodies, we visualized for light microscopy analyses immunoreactive elements by treating the sections with ABC followed by DAB using Peroxidase Stain DAB kits (Nacalai Tesque Japan). PS199 and anti- α -tubulin were used as primary antibodies for confocal laser microscopy analyses. Immunoreactive elements were visualized with Alexa568-conjugated anti-mouse IgG and Alexa488-conjugated anti-rabbit IgG, and then examined with a Radiance 2000 KR3 confocal microscope (Bio-Rad). We stained some sections with Congo red and Thioflavin T, which recognize the β -sheet structure of tau fibrils, and then examined them with a light microscope equipped with crossed polarizing filters (Nikon). NFTs were identified using a standard Gallyas silver-impregnation method, which is used to assess structural changes of the brain in AD (22).

RESULTS

The A β levels in the brains of mPS1 knock-in mice were quantified by sandwich enzyme-linked immunoassay (23) and Western blot analysis. Similar to a previous report (19), the level of A β_{1-42} was elevated in the brains of mPS1 mice compared with that in the brains of wild-type mice (wPS1 mice). Most of the A β_{1-40} and A β_{1-42} was recovered in the Triton X-100-soluble fraction, and very little was recovered in the 1% SDS-insoluble fraction, suggesting that neither A β_{1-40} nor A β_{1-42} aggregated and deposited within the brains of the mPS1 mice. Moreover, A β immunostaining in tissue sections was absent, suggesting again that neither extracellular nor intracellular A β accumulated *in vivo* (data not shown). Thus, murine A β failed to deposit in the brains of mPS1 mice, even though A β_{1-42} levels in these brains increased.

Characterization of NFT-like Pathology in Mutant PS1 Mice—Five-month-old heterozygous mPS1 mice exhibited no pathological changes (Fig. 1A); however, in 7-month-old or older mice, we detected phospho-tau accumulation (PS199) in neurons in the hippocampal region (Fig. 1B). The prevalence and distribution of these PS199-positive neurons gradually increased and widened, respectively, with age, and in 14–16-month-old mice, we observed phospho-tau immunoreactivity in hippocampal CA3 neurons (Fig. 1D). By contrast, wPS1 mice did not show this pattern of phospho-tau immunoreactivity (Fig. 1, C and D). Alz50, an antibody that recognizes the conformational change of tau in PHF-tau, also labeled CA3 neurons (Fig. 1, E–G). In summary, these findings indicate that heterozygous mPS1 mice, whose alleles most precisely reflect the genotype of humans bearing this mutation, exhibited phospho-tau accumulation with PHF-tau epitopes, whereas wPS1 mice of the same age showed no sign of tau accumulation.

Data related to the other histological criteria for NFTs confirmed these findings. In heterozygous mPS1 mice, we observed Congo red birefringence (Fig. 1, H–J) and Thioflavin T reactivity (Fig. 1K) in hippocampal neurons. The Gallyas silver staining method revealed argyrophillic neurons in the hippocampus of mPS1 mice (Fig. 1L). Argyrophillic and Congo red-positive neurons were less numerous than phospho-tau-positive neurons (less than 5% of phospho-tau-positive neurons). The tau-accumulating neurons of these mice also exhibited reduced α -tubulin immunoreactivity (Fig. 1, M and N) similar to that displayed by NFT-bearing neurons. As we previously showed in tau Tg mice (24, 25), weaker α -tubulin immunoreactivity might indicate destruction of microtubules in tau-accumulating neurons in the mPS1 mice. TUNEL staining, however, revealed no signs of apoptosis in these neurons (Fig. 1, O–R). Taken together, these results suggest that mPS1 affects the cytoskeleton of hippocampal neurons and induces NFT-like accumulation of hyperphosphorylated tau.

Biochemical and Ultrastructural Analysis of Tau in Mutant PS1 Mice—We confirmed the accumulation of NFT-like tau in mPS1 mice with biochemical and electron microscopy analyses. Because tau becomes detergent insoluble when aggregated, we assessed the amount of tau in the SDS-insoluble fraction derived from the brains of mPS1 mice. As shown in Fig. 2A, small amounts of tau were recovered in the SDS-insoluble fraction from 2-month-old mPS1 mice. The amount of tau recovered in the SDS-insoluble fraction increased with aging, and a large amount of tau was recovered from 14-month-old heterozygous mPS1 mice compared with age-matched wPS1 mice. (The amount of SDS-insoluble tau in mPS1 mice was ~2% of the total tau in these mice).

We also investigated the amount of SDS-insoluble tau in different brain regions of mPS1 mice. Tau was recovered from the hippocampus, and small amounts were recovered from the cerebral cortex, striatum, and cerebellum. This might be explained by the inverse correlation of NFT with pin1 expression (26).

Tau Inclusions in FAD Mutant PS1 Knock-in Mice

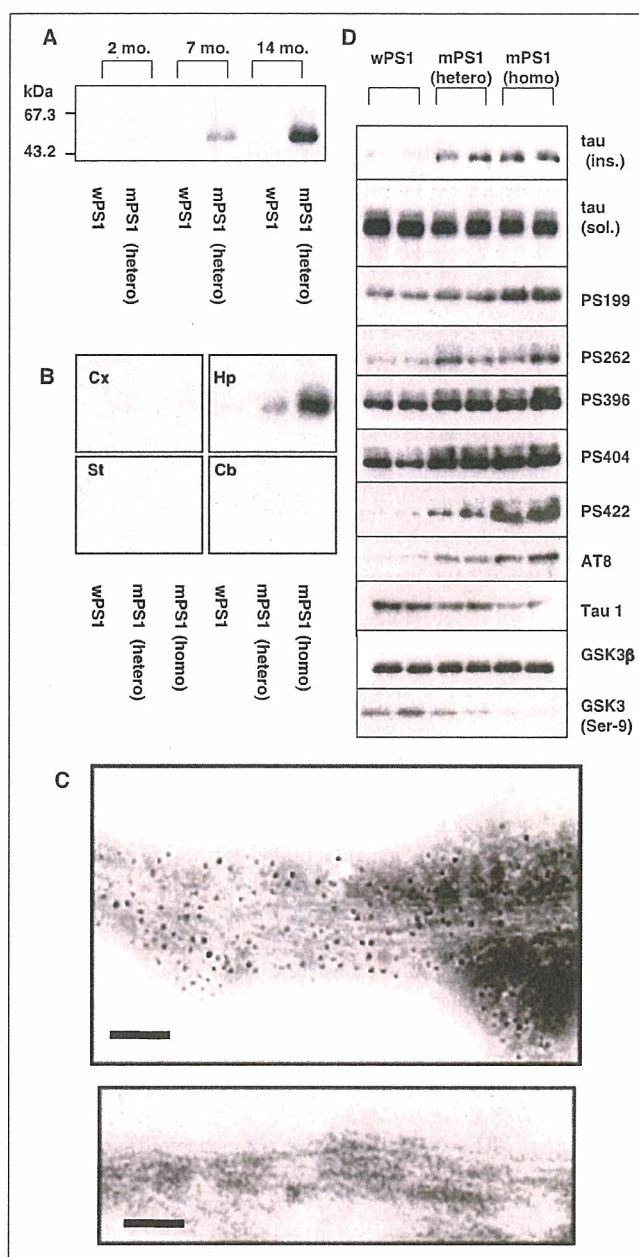


FIGURE 2. Biochemical and electron microscopy (EM) analyses of mPS1 mice. A, SDS-insoluble tau from the brains of 2-, 7-, and 14-month-old heterozygous mPS1 mice. B, SDS-insoluble tau in micro-dissected cortex (Cx), hippocampus (Hp), brainstem (St), and cerebellum (Cb) of 12-month-old wild-type PS1, heterozygous mPS1, and homozygous mPS1 mice. C, immuno-EM analysis of SDS-insoluble materials from 12-month-old heterozygous mPS1 mice. Fibrils labeled with 5-nm gold particles indicate immunoreactivity to the phosphorylation-independent tau antibody, JM (upper panel). Immunogold labeling was not observed on fibrils (control) stained in the absence of primary antibody (lower panel). Scale bars: 100 nm. D, Western blots containing SDS-insoluble and RIPA-soluble materials from the hippocampi of 14-month-old wPS1, heterozygous mPS1, and homozygous mPS1 mice. (Lane pairs correspond to a set of two mice per mouse strain.) Order of blots (from top to bottom): SDS-insoluble tau (*tau (ins.)*); RIPA-soluble tau (*tau (sol.)*); RIPA-soluble phosphorylated tau (PS199, PS262, PS396, PS404, PS422, and AT8); unphosphorylated tau (*Tau 1*), active GSK3 β (GSK3 β); and inactive GSK3 β (GSK3 β Ser-9).

The SDS-insoluble material recovered from mPS1 mice were further investigated with electron microscopy. As shown in Fig. 2C, tau-positive fibrils were detected in the SDS-insoluble fraction. These fibrils appeared to be straight tubules, about 10 nm in diameter. The biochem-

Tau Inclusions in FAD Mutant PS1 Knock-in Mice

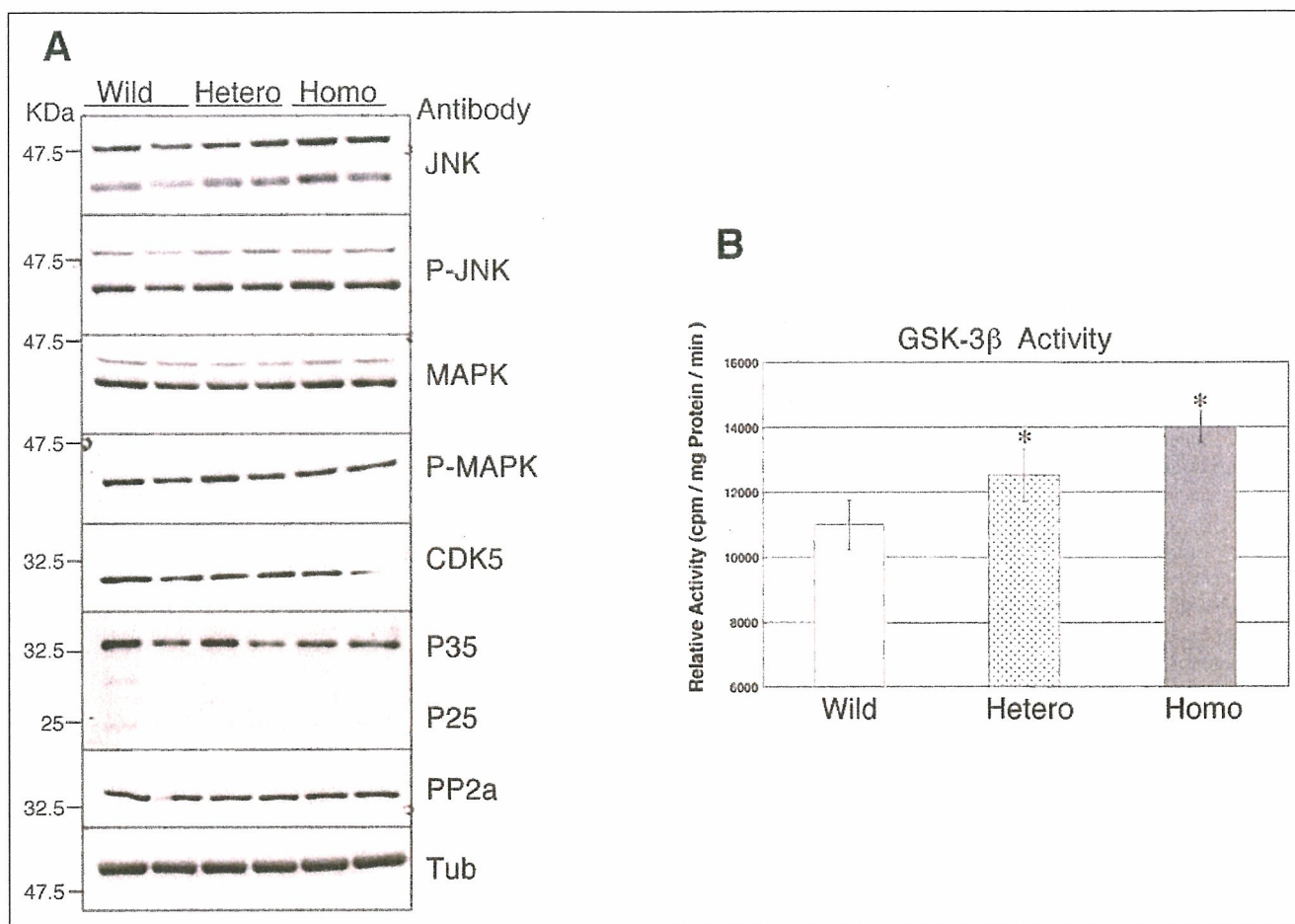


FIGURE 3. Tau kinase activity in 12-month-old mPS1 mice. A, hippocampal lysates from wPS1, heterozygous mPS1, and homozygous mPS1 mice were analyzed with Western blotting and antibodies against tau kinases and phosphatases: total JNK (*JNK*); phospho-JNK (*P-JNK*); MAP kinase (*MAPK*); phosphorylated MAP kinase (*PMAPK*); CDK5; the CDK5 activators, p35 and p25; and phosphatase 2a (*PP2a*). A blot stained with anti-tubulin antibody (*Tub*) represents the control. B, *GSK-3β* activity in immunoprecipitated brain samples derived from wPS1, heterozygous mPS1, and homozygous mPS1 mice were determined with an assay that measures the incorporation of ^{32}P into a *GSK-3β* substrate peptide. Data are expressed as averages \pm S.D. (*, $p < 0.05$; $n = 3$).

ical and ultrastructural analyses strongly suggest that NFT-like tau aggregation formed primarily in hippocampal neurons of mPS1 mice.

The NFTs found in AD brains contain highly phosphorylated tau (27). Hyperphosphorylation of tau leads to the formation of fibrillar tau (28). To determine whether tau hyperphosphorylation also occurs in mPS1 mice, we examined the extent of tau phosphorylation in 14-month-old wPS1, heterozygous mPS1, and homozygous mPS1 mice (Fig. 2D). Immunoblotting with various phosphorylation-dependent anti-tau antibodies revealed that the amount of SDS-insoluble tau was nearly the same in heterozygous and homozygous mPS1 mice (Fig. 2D, *tau(ins.)*). This amount, however, was greater than that in wPS1 mice. Although the total amounts of tau in soluble fractions from the three types of mice were similar (*i.e.* bands had slower mobility than the unphosphorylated Tau-1-immunoreactive band) (Fig. 2D, *tau(sol.)*), the amounts of phosphorylated tau immunostained by PS199, PS262, PS396, PS404, PS422, and AT8 were elevated in the heterozygous and homozygous mPS1 mice compared with those in the wPS1 mice. The extent of tau phosphorylation at the AT8, PS422, and PS199 epitopes appeared to depend on the number of mPS1 alleles present in the mice, as shown by the comparatively greater immunosignal intensity of samples derived from homozygous than in heterozygous mPS1 mice, suggesting that mPS1 expression affects the hyperphosphorylation of tau. The immunostaining intensity of Tau-1, an antibody that recognizes

unphosphorylated tau, also correlated with genotype. Tau-1 immunoreactivity was greater in samples derived from wPS1 mice than in heterozygous and homozygous mPS1 mice (wPS1 > heterozygous mPS1 > homozygous mPS1), confirming that mPS1 induced the hyperphosphorylation of tau.

GSK-3β, Tau Kinase, and Tau Phosphatase Activity—Activation of *GSK-3β*, a known tau kinase, was also associated with mPS1 genotype. Although total *GSK-3β* levels were similar among wPS1, heterozygous mPS1, and homozygous mPS1 mice, inactive *GSK-3β* (*GSK-3β* phosphorylated at Ser-9) levels varied inversely with the number of mPS1 alleles present (Fig. 2D; *GSK3β* and *GSK3β(Ser-9)*). This inverse correlation was confirmed by comparing the *GSK-3β* activity in immunoprecipitated brain samples derived from wPS1, heterozygous mPS1, and homozygous mPS1 mice (Fig. 3B). This assay revealed elevated *GSK-3β* activity in heterozygous mPS1 compared with wPS1 mice ($p < 0.05$; $n = 3$), and also in homozygous mPS1 mice compared with heterozygous mice ($p < 0.05$; $n = 3$). Taken together, we conclude that the mutant PS1 activated *GSK-3β*, thereby enhancing tau phosphorylation and resulting in the formation of NFT-like tau aggregates (Figs. 1 and 2). These results support those from a previous report (20).

We also investigated how other kinases and phosphatases may contribute to tau phosphorylation in mPS1 mice. As shown in Fig. 3A, levels of the active forms of phosphorylated JNK; phosphorylated MAP kinase; CDK5;

the CDK5 activators p35 and p25; and PP2a were similar among wPS1, heterozygous mPS1, and homozygous mPS1 mice, indicating that the tau phosphorylation mediated by these enzymes are not affected by the PS1 mutation. Nonetheless, other mechanisms are expected to be involved in the mPS1-induced hyperphosphorylation of tau, because GSK-3 β alone cannot phosphorylate all of the phosphorylation sites in tau.

DISCUSSION

In the present study, we demonstrated that the brains of mice harboring a PS1 mutation accumulated NFT-like phospho-tau. Biochemical analysis of SDS-insoluble tau revealed tau fibrils. These NFT-like tau inclusions were similar to those observed in FTDP-17 mutant tau transgenic mice (24, 25, 28), in mice overexpressing p25, a CDK5 activator (29), and in Pin1 knock-out mice (26). The neurons of other PS1 knock-in and mutant PS1 transgenic mice; however, failed to show cytoskeletal changes (30, 31). To create their mutant PS1 knock-in mice, Guo *et al.* (32) used a hybrid mouse composed of 129SV and C57BL6 strains, whereas in the present study we used mice resulting from 10 generations of crossbreeding with C57BL6 mice. The genetic background of our mice, which is most likely to be different from the backgrounds of mice used in previously studies, could have influenced how the PS1 mutation contributed to NFT formation and cytoskeletal changes. Another possible explanation for the apparent discrepancy between our findings and others is that our PS1 knock-in mice harbored a different PS1 mutation from that harbored by mutant PS1 knock-in mice developed by other laboratories.

Previously, we found certain PS1 mutations that increase A β ₁₋₄₂ levels are poor predictors for the onset of FAD (5). Our present results, however, suggest that the accumulation of NFT-like tau could determine the onset of AD. These two differing outcomes would also explain why some PS1 mutations accelerate NFT formation and neuronal loss without accelerating A β deposition (18). Thus, PS1 mutations that accelerate both NFT formation and A β ₁₋₄₂ production may further accelerate related neuropathologies, suggesting that the cause of early onset AD may be related to a PS1 mutation.

The mechanism underlying the mutant PS1-associated accumulation of NFTs may involve the activation of GSK-3 β . Our results indicate that GSK-3 β is activated in our mPS1 knock-in mice; this is consistent with other mPS1 transgenic mice. Recently, wild-type PS1 has been shown to activate PI3 kinase/Akt signaling by promoting the association of cadherin and PI 3-kinase, whereas mutant PS1 was unable to do so (32). Thus, mutant PS1 appears to impair PI 3-kinase/Akt signaling by affecting selected signaling receptors (33) or by reducing cadherin/PI3 kinase association (32), which eventually leads to the activation of GSK-3 β . Whereas the mutant PS1-associated activation of GSK-3 β occurred in young mice, tau accumulation occurred only later on in older mice. This led us to hypothesize that, by some mechanism, phosphorylated tau degrades before it aggregates. This unknown mechanism is then inactivated during aging, leading to the accumulation and aggregation of tau that occurs in aged individuals.

Patients harboring the FAD mutation of PS1 develop AD with 100% penetration. Based on our results, we propose that the PS1 mutation in FAD leads to the early onset of AD through the activation of GSK-3 β , which leads to NFT formation and the loss of neurons and synapses. Moreover, we believe that the rate of GSK-3 β activation is accelerated by extracellular A β oligomers. The exact molecular mechanism mediating the mutant PS1-induced activation of GSK-3 β requires clarification to further our understanding of how AD develops.

REFERENCES

- Sherrington, R., Rogaev, E. I., Liang, Y., Rogaeva, E. A., Levesque, G., Ikeda, M., Chi, H., Lin, C., Li, G., Holman, K., Tsuda, T., Mar, L., Foncin, J.-F., Bruni, A. C., Montesi,

Tau Inclusions in FAD Mutant PS1 Knock-in Mice

- M. P., Sorbi, S., Rainero, I., Pinessi, L., Nee, L., Chumakov, I., Pollen, D., Brookes, A., Sanseau, P., Polinsky, R. J., Wasco, W., Da Silva, H. A. R., Haines, J. L., Pericak-Vance, M. A., Tanzi, R. E., Roses, A. D., Fraser, P. E., Rommens, J. M., and St. George-Hyslop, P. H. (1995) *Nature* **375**, 754–760
- Cruts, M., Backhovens, H., Wang, S. Y., Van Gassen, G., Theuns, J., De Jonghe, C. D., Wehnert, A., De Voecht, J., De Winter, G., and Cras, P. (1995) *Hum. Mol. Genet.* **4**, 2363–2371
- St George-Hyslop, P. H., and Petit, A. (2005) *C. R. Biol.* **328**, 119–130
- St George-Hyslop, P. H. (2000) *Biol. Psychiatry* **47**, 183–199
- Murayama, O., Honda, T., Mercken, M., Murayama, M., Yasutake, K., Nihonmatsu, N., Nakazato, Y., Michel, G., Song, S., Sato, K., Takahashi, H., and Takashima, A. (1997) *Neurosci. Lett.* **229**, 61–64
- Scheuner, D., Eckman, C., Jensen, M., Song, X., Citron, M., Suzuki, N., Bird, T. D., Hardy, J., Hutton, M., Kukull, W., Larson, E., Levy-Lahad, E., Viitanen, M., Peskind, E., Poorkaj, P., Schellenberg, G., Tanzi, R., Wasco, W., Lannfelt, L., Selkoe, D., and Younkin, S. (1996) *Nat. Med.* **2**, 864–870
- Holcomb, L., Gordon, M. N., McGowan, E., Yu, X., Benkovic, S., Jantzen, P., Wright, K., Saad, I., Mueller, R., Morgan, D., Sanders, S., Zehr, C., O'Campo, K., Hardy, J., Prada, C. M., Eckman, C., Younkin, S., Wilson, M. A., Younkin, S., Kandel, E. R., Kirkwood, A., and Shen, J. (2001) *Neuron* **31**, 713–726
- Amtul, Z., Lewis, P. A., Piper, S., Crook, R., Baker, M., Findlay, K., Singleton, A., Hogg, M., Younkin, L., Younkin, S. G., Hardy, J., Hutton, M., Boeve, B. F., Tang-Wai, D., and Golde, T. E. (2002) *Neurobiol. Dis.* **9**, 269–273
- Dermaut, B., Kumar-Singh, S., Engelborghs, S., Theuns, J., Rademakers, R., Saerens, J., Pickut, B. A., Peeters, K., van den Broeck, M., Vennekens, K., Claes, S., Cruts, M., Cras, P., Martin, J. J., Van Broeckhoven, C., and De Deyn, P. P. (2004) *Ann. Neurol.* **55**, 617–626
- Tang-Wai, D., Lewis, P., Boeve, B., Hutton, M., Golde, T., Baker, M., Hardy, J., Michels, V., Ivnik, R., Jack, C., and Petersen, R. (2002) *Dement. Geriatr. Cogn. Disord.* **14**, 13–21
- Evin, G., Smith, M. J., Tziotis, A., McLean, C., Canterford, L., Sharples, R. A., Cappai, R., Weidemann, A., Beyreuther, K., Cotton, R. G., Masters, C. L., and Culvenor, J. G. (2002) *Neuroreport* **13**, 719–723
- Yoshiyama, Y., Lee, V. M., and Trojanowski, J. Q. (2001) *Curr. Neurol. Neurosci. Rep.* **1**, 413–421
- Gomez-Isla, T., Growdon, W. B., McNamara, M. J., Nochlin, D., Bird, T. D., Arango, J. C., Lopera, F., Kosik, K. S., Lantos, P. L., Cairns, N. J., and Hyman, B. T. (1999) *Brain* **122**, 1709–1719
- Nakano, Y., Kondoh, G., Kudo, T., Imaizumi, K., Kato, M., Miyazaki, J. I., Tohyama, M., Takeda, J., and Takeda, M. (1999) *Eur. J. Neurosci.* **11**, 2577–2581
- Takahashima, A., Murayama, M., Murayama, O., Kohno, T., Honda, T., Yasutake, K., Nihonmatsu, N., Mercken, M., Yamaguchi, H., Sugihara, S., and Wolozin, B. (1998) *Proc. Natl. Acad. Sci. U. S. A.* **95**, 9637–9641
- Van Lint, J., Khandelwal, R. L., Merlevede, W., and Vandenheede, J. R. (1993) *Anal. Biochem.* **208**, 132–137
- Iqbal, K., Braak, E., Braak, H., Zaidi, T., and Grundke-Iqbal, I. (1991) *Neurobiol. Aging* **12**, 357–361
- Sun, X., Cole, G. M., Chu, T., Xia, W., Galasko, D., Yamaguchi, H., Tanemura, K., Frautschy, S. A., and Takashima, A. (2002) *Neurobiol. Aging* **23**, 195–203
- Tatebayashi, Y., Miyasaka, T., Chui, D. H., Akagi, T., Mishima, K., Iwasaki, K., Fujiwara, M., Tanemura, K., Murayama, M., Ishiguro, K., Planel, E., Sato, S., Hashikawa, T., and Takashima, A. (2002) *Proc. Natl. Acad. Sci. U. S. A.* **99**, 13896–13901
- Tanemura, K., Murayama, M., Akagi, T., Hashikawa, T., Tominaga, T., Ichikawa, M., Yamaguchi, H., and Takashima, A. (2002) *J. Neurosci.* **22**, 133–141
- Liou, Y. C., Sun, A., Ryo, A., Zhou, X. Z., Yu, Z. X., Huang, H. K., Uchida, T., Bronson, R., Bing, G., Li, X., Hunter, T., and Lu, K. P. (2003) *Nature* **424**, 556–561
- Lee, V. M., Balin, B. J., Otvos, L., Jr., and Trojanowski, J. Q. (1991) *Science* **251**, 675–678
- Sato, S., Tatebayashi, Y., Akagi, T., Chui, D. H., Murayama, M., Miyasaka, T., Planel, E., Tanemura, K., Sun, X., Hashikawa, T., Yoshioka, K., Ishiguro, K., and Takashima, A. (2002) *J. Biol. Chem.* **277**, 42060–42065
- Cruz, J. C., Tseng, H. C., Goldman, J. A., Shih, H., and Tsai, L. H. (2003) *Neuron* **40**, 471–483
- Siman, R., Reaume, A. G., Savage, M. J., Trusko, S., Lin, Y. G., Scott, R. W., and Flood, D. G. (2000) *J. Neurosci.* **20**, 8717–8726
- Guo, Q., Sebastian, L., Sopher, B. L., Miller, M. W., Ware, C. B., Martin, G. M., and Mattson, M. P. (1999) *J. Neurochem.* **72**, 1019–1029
- Baki, L., Shioi, J., Wen, P., Shao, Z., Schwarzman, A., Gama-Sosa, M., Neve, R., and Robakis, N. K. (2004) *EMBO J.* **23**, 2586–2596
- Kang, D. E., Sang Yoon, I., Repetto, E., Busse, T., Yermian, N., Ie, L., and Koo, E. H. (2005) *J. Biol. Chem.* **280**, 31537–31547

Methyl-CpG Binding Proteins Are Involved in Restricting Differentiation Plasticity in Neurons

Hiroki Setoguchi, Masakazu Namihira, Jun Kohyama, Hirotsugu Asano, Tsukasa Sanosaka, and Kinichi Nakashima*

Laboratory of Molecular Neuroscience, Graduate School of Biological Sciences, Nara Institute of Science and Technology, Nara, Japan

Neurons and astrocytes are generated from common neural precursors, yet neurogenesis precedes astrocytogenesis, which normally commences at later stages of development. We have previously reported that a particular cytosine residue within a STAT3-binding site in the astrocyte-specific marker glial fibrillary acidic protein (GFAP) gene promoter becomes demethylated in neuroepithelial cells as gestation proceeds. This demethylation correlates tightly with the onset of astrocyte differentiation, suggesting that a change in DNA methylation at cell-type-specific gene promoters controls the switch from neurogenesis to astrocytogenesis in the developing brain. Here, we show that late-gestation neuroepithelial cells, which have already lost the methylation in the STAT3-binding site within the GFAP promoter, can still give rise to neurons and that these neurons do not respond to a STAT3-activating cytokine to express GFAP. Members of a transcriptional repressor family, the methylated-CpG binding proteins (MBDs), including MeCP2, are predominantly expressed in neurons, and ectopic MeCP2 expression inhibited astrocyte differentiation of neuroepithelial cells. Moreover, we found that exon 1 of the GFAP gene remains hypermethylated even in neuroepithelial cells at a late developmental stage and in neurons differentiated from such neuroepithelial cells. We further demonstrate that MeCP2 actually binds to the highly methylated exon 1 of the GFAP gene in neurons. These results suggest that region-specific DNA methylation and MBDs play an important role in the regulation of differentiation plasticity in neurons. © 2006 Wiley-Liss, Inc.

Key words: neural stem cell; neuron; epigenetics; plasticity; MBD

The mammalian central nervous system (CNS) is established through a temporally and spatially well-organized sequence of events during development. Multipotent neural stem cells (NSCs) are defined as cells that can self-renew and give rise to the three major CNS cell types (neurons, astrocytes, and oligodendrocytes). However, NSCs lack multipotentiality in early gestation and differentiate only into neurons at midgestation (Qian

et al., 2000; Sauvageot and Stiles, 2002). NSCs gradually acquire multipotentiality and start to differentiate into astrocytes and oligodendrocytes during late gestation (Qian et al., 2000; Sauvageot and Stiles, 2002). Although the mechanisms of NSC fate determination are not fully understood, it is becoming apparent that both extracellular cues, including cytokine signaling and intracellular programs such as epigenetic gene regulation, are deeply involved in the fate specification of NSCs (Edlund and Jessell, 1999; Takizawa et al., 2001; Hsieh and Gage, 2004; Abematsu et al., 2006).

The Janus kinase (JAK)-signal transducer and activator of transcription (STAT) pathway, which is activated by the cytokine leukemia inhibitory factor (LIF) through its heterodimeric receptor complex, LIFR β and gp130, can effectively induce astrocyte differentiation (Bonni et al., 1997; Rajan and McKay, 1998). Bone morphogenetic proteins (BMPs) also activate expression of astrocytic genes via complex formation between the BMP-downstream transcription factor Smad1 and STATs, bridged by the transcription coactivator p300/CBP (Naka-

The first two authors contributed equally to this work.

Supplementary Material for this article is available online at [http://www.mrw.interscience.wiley.com/suppmat/0360-4012/suppmat/\(www.interscience.wiley.com\)](http://www.mrw.interscience.wiley.com/suppmat/0360-4012/suppmat/(www.interscience.wiley.com)).

Contract grant sponsor: Grant-in-Aid for Young Scientists from Japan Society for the Promotion of Science (JSPS); Contract grant sponsor: Grant-in-Aid for Exploratory Research from Japan Society for the Promotion of Science (JSPS); Contract grant sponsor: Grant-in-Aid for Scientific Research on Priority Areas from the Ministry of Education, Culture, Sports, Science and Technology; Contract grant sponsor: Kato Memorial Bioscience Foundation; Contract grant sponsor: Uehara Memorial Foundation; Contract grant sponsor: Nakajima Foundation; Contract grant sponsor: Naito Foundation and the Foundation for Nara Institute of Science and Technology.

*Correspondence to: Kinichi Nakashima, PhD, Laboratory of Molecular Neuroscience, Graduate School of Biological Sciences, Nara Institute of Science and Technology, 8916-5 Takayama, Nara 630-0101, Japan. E-mail: kin@bs.naist.jp

Received 2 May 2006; Revised 11 May 2006; Accepted 4 June 2006

Published online 31 July 2006 in Wiley InterScience (www.interscience.wiley.com). DOI: 10.1002/jnr.21001

shima et al., 1999b; Sun et al., 2001). Gene knockouts of LIF (Bugga et al., 1998), LIFR β (Koblar et al., 1998), gp130 (Nakashima et al., 1999a), and STAT3 (He et al., 2005) all result in impaired astrocyte differentiation *in vivo*, further indicating that JAK-STAT signaling contributes to astroglialogenesis in the developing CNS.

Cell-intrinsic programs regulating fate determination of NSCs include epigenetic modifications such as chromatin remodeling and DNA methylation. The cytosine residue in CpG dinucleotides of vertebrate genomes is a well-known target for DNA methylation, leading to suppression of methylated genes. Establishment of the proper gene methylation patterns is essential for inactivation of the X chromosome, genomic imprinting, and normal development; abnormalities in DNA methylation are frequently associated with tumorigenesis (Jones and Baylin, 2002), with cell aging (Issa et al., 1994), and with several neurological disorders, including Rett (RTT), immunodeficiency-centromeric instability-facial anomalies (ICF), fragile-X, and α -thalassemia mental retardation (ATR-X) syndromes (Robertson and Wolffe, 2000).

Mechanistically, DNA methylation is considered to elicit its effects by interfering with binding of transcriptional factors to their cognate recognition sequences (Watt and Molloy, 1988) or by creating a binding site for members of a transcriptional repressor family, the methyl-CpG binding proteins (MBDs), that recognize methylated CpG sites (Hendrich and Bird, 1998). We have previously shown that a CpG dinucleotide within a STAT3-binding element (TTCCGAGAA) in the astrocytic marker glial fibrillary acidic protein (GFAP) gene promoter is highly methylated in neuroepithelial cells at midgestation, when the cells differentiate only into neurons and not into astrocytes. Because STAT3 does not bind to the methylated recognition sequence, neuroepithelial cells at midgestation do not express GFAP even when stimulated by the STAT3-activating cytokine LIF. At a later developmental stage, the STAT3 site becomes demethylated in neuroepithelial cells, which can then express GFAP in response to LIF stimulation. We suggested, based on these findings, that DNA methylation is a critical cell-intrinsic determinant of astrocyte differentiation during brain development. However, neuroepithelial cells at the late-gestation stage can still become neurons, even though they have already lost the methylation at the STAT3-binding site (Takizawa et al., 2001). Thus, it remains unclear whether neurons produced from neuroepithelial cells at late gestation express astrocyte-specific genes in response to STAT3-activating cytokines. Moreover, little is known about how neural cells maintain their cellular identity, for example, by sustaining and/or suppressing the expression of cell type-restricted genes.

It has been reported that epigenetic mechanisms are likely used to regulate cellular differentiation plasticity (Bird, 2002). Programmed changes in DNA methylation are essential features of development, and their disruption frequently results in developmental abnormality (Li et al., 1992). The nervous system appears particularly vulnerable to epigenetic changes, as indicated by, for

instance, widespread CNS defects in RTT, a postnatal neurodevelopmental disorder caused by mutations in an MBD gene, MeCP2. RTT is characterized by the loss of acquired motor and language skills, autistic features, and unusual stereotyped movements (Kriaucionis and Bird, 2003). Disruption of the MBD1 gene also results in misregulation of neurogenesis in the adult hippocampus (Zhao et al., 2003). DNA methyltransferase (DNMT) 1 and MBDs are implicated in the differential vulnerability of cortical neurons to resist cell death following ischemia or kindling (Endres et al., 2000; Jung et al., 2002). Thus, although DNA methylation and MBDs play crucial roles in the development and/or function of the CNS, their roles in the fate specification of NSCs and regulation of neural cell plasticity remain to be fully elucidated.

Here, we report that DNA methylation and MBDs are involved in the silencing of astrocytic genes in neurons and that ectopic expression of MBDs indeed inhibits astrocyte differentiation of neuroepithelial cells, which normally differentiate into astrocytes under the control of STAT3-activating cytokines. We show that the exon1 region of the GFAP gene is kept highly methylated, even in neuroepithelial cells that have already lost the methylation in the STAT3-binding site within the GFAP promoter and in neurons generated from these cells. Furthermore, MeCP2 is expressed exclusively in neurons and actually binds to the highly methylated GFAP exon 1. In addition to GFAP, MeCP2 can bind to hypermethylated CpG sites around the transcriptional start site of another astrocytic marker, the S100 β gene, to suppress its expression. MBD1, like MeCP2, inhibits astrocyte differentiation of neuroepithelial cells, suggesting some functional redundancy among MBDs. These results imply that region-specific DNA methylation and MBDs play an important role in the regulation of differentiation plasticity to maintain the integrity of neurons.

MATERIALS AND METHODS

Neuroepithelial Cell Culture

Time-pregnant ICR mice were used to prepare neuroepithelial cells. The experimental protocols described below were performed according to the animal experimentation guidelines of Nara Institute of Science and Technology. Neuroepithelial cells were prepared from telencephalons of E14.5 mice and cultured as described previously (Nakashima et al., 1999b). Briefly, the telencephalons were triturated in Hank's balanced salt solution (HBSS) by mild pipetting with a 1-ml pipet tip (Gilson). Dissociated cells were cultured for 4 days in N2-supplemented Dulbecco's modified Eagle's medium with F12 (Gibco, Grand Island, NY) containing 10 ng/ml basic fibroblast growth factor (bFGF; R&D Systems, Minneapolis, MN; N2/DMEM/F12/bFGF) on culture dishes that had been precoated with poly-L-ornithine (Sigma, St. Louis, MO) and fibronectin (Sigma). To obtain differentiated cells, neuroepithelial cells were cultured in differentiation medium [growth medium with 0.5% fetal bovine serum (FBS), but without bFGF] for 4 days.

Immunocytochemistry

Cells cultured on coated chamber slides (Nunc) were washed with phosphate-buffered saline (PBS), fixed in 4% paraformaldehyde in PBS, and stained with one of the following primary antibodies: rabbit anti-MeCP2 (1:100; Santa Cruz Biotechnology, Santa Cruz, CA), rabbit anti-GFP (1:1000; MBL), mouse anti- β III-tubulin (Tuj-1; 1:500; Sigma), mouse antimicrotubule-associated proteins 2a and 2b (MAP2ab; 1:250; Sigma), mouse anti-NeuN (1:100; Chemicon, Temecula, CA), guinea pig anti-GFAP (1:2,500; Advanced Immunochemical), or mouse anti-S100 β (1:500; Sigma). The following secondary antibodies were used: Alexa488-conjugated goat anti-mouse IgG (1:500; Molecular Probes, Eugene, OR) or Cy3-conjugated goat anti-mouse IgG (1:500; Chemicon), Alexa488-conjugated goat anti-rabbit (1:500; Molecular Probes) or rhodamine-conjugated donkey anti-rabbit (1:250; Chemicon), and Cy5-conjugated donkey anti-guinea pig (1:250; Chemicon). Nuclei were stained by using bisbenzimidazole H33258 fluorochrome trihydrochloride (Nacalai Tesque). All experiments were independently replicated at least three times.

Recombinant Retrovirus Construction and Infection

The rat MBD1 and MeCP2 cDNAs were cloned into the expression vector pMY containing an internal ribosome entry site followed by upstream of the GFP gene (Morita et al., 2000). The Plat-E packaging cell line was transiently transfected with retrovirus DNA by Trans-IT 293 (Mirus, Madison, WI) (Morita et al., 2000). On the following day, the medium was replaced with N2/DMEM/F12/bFGF, and the cells were cultured in this medium for 1 day before virus was collected.

Bisulfite Sequencing

Sodium bisulfite treatment of genomic DNA was performed essentially as described previously (Clark et al., 1994). Briefly, 5 μ g genomic DNA was digested with HindIII and EcoRI, denatured with 0.3 M NaOH at 37°C for 15 min, and incubated with 3.1 M sodium bisulfite and 0.5 mM hydroquinone at 55°C for 16 hr. The samples were purified by using a desalting column (Promega, Madison, WI) according to the manufacturer's instructions and eluted in 50 μ l H₂O. Three molar NaOH (5.5 μ l) was added, and the samples were incubated at 37°C for 15 min. Samples were then neutralized by the addition of 3 M ammonium acetate, ethanol precipitated, and dissolved in H₂O. Specific DNA fragments were amplified by PCR with the following sets of primers: for the STAT3 recognition sequence-containing region in the GFAP promoter, GFmS (5'-GGGATTTATTAGGAGAATTTTAGTAAAGTAG-3') and GFmAS (5'-TCTACCCATACTTAACTTCTAATATCTAC-3'); for the exon 1 region in the GFAP gene, GFmeEx1S (5'-GATAGGTAAGTAATTTATGGA-3') and GFmeEx1AS (5'-TTCAATCTCTACTCACTAACC-3'); and, for the proximal region of the transcriptional start site in the S100 β gene, S100BmeS (5'-AGTTTTTAGTATTTAGTATGAG-3') and S100BmeAS (5'-TCTCTTAAATCCTATCAATAAC-3'). The PCR products were cloned into pT7Blue vector (Novagen), and 10–19 randomly selected clones were sequenced.

Chromatin Immunoprecipitation Assay

Chromatin immunoprecipitation (ChIP) was performed according to a protocol published by Upstate Biotechnology (Lake Placid, NY). Undifferentiated neuroepithelial cells and differentiated cells were exposed to formaldehyde, at a final concentration of 1% added directly to the tissue culture medium. Coimmunoprecipitated DNA was used as a template for PCR with the following sets of primers: for the exon 1 region in the GFAP gene, GFex1S (5'-TGACATCCCAGGAGCCAG-3') and GFex1AS (5'-CAGTCTCTCTGCTCACTAGCC-3'); and, for the proximal region of the transcriptional start site in the S100 β gene, S100BchipS (5'-CTCTACACTTCCTACCCAA-CAG-3') and S100BchipAS (5'-GTTTTCTCTTGGGTCCT-GTCAG-3'). Antibody used for the ChIP assay was rabbit anti-MeCP2 (Upstate Biotechnology).

RESULTS

Neurons Generated From Neuroepithelial Cells at Late Gestation Do Not Express GFAP Even When Stimulated With an Astrocyte-Inducing Cytokine

It has been shown that neuroepithelial cells at midgestation (E11.5) do not respond to LIF to express GFAP and that this is attributable to the hypermethylation status of the STAT3-binding site in the GFAP promoter (Takizawa et al., 2001; Doetsch, 2003). However, neuroepithelial cells at relatively late gestation (E14.5), which have already lost the methylation, can still produce neurons. Therefore, we first sought to examine whether neurons that had differentiated from such cells expressed GFAP in response to LIF stimulation. Primary E14.5 neuroepithelial cells cultured for 4 days in the presence of bFGF were subsequently incubated without bFGF but in the presence of 0.5% FBS to induce spontaneous differentiation. Under these culture conditions, over 30% of the cells became positive for the neuronal marker Tuj-1 (Fig. 1A). After 4 days' induction of differentiation, the cells were treated with LIF for an additional 4 days. Tuj-1-positive neurons remained GFAP negative, regardless of the 4-day LIF stimulation (Fig. 1B,C). The number of Tuj-1-positive cells before and after LIF stimulation was not significantly different (Fig. 1D), suggesting that differentiated neurons could not become Tuj-1-negative/GFAP-positive cells. In addition, we confirmed the accumulation of tyrosine-phosphorylated STAT3 in the nuclei of neurons in response to LIF stimulation (Supplemental Fig. 1). To exclude the possibility that the suppression of GFAP expression in neurons is due to remethylation of the STAT3-binding sequence in the promoter, we analyzed the methylation status of CpG sites in the region between -1,622 bp and -1,423 bp of the promoter, which includes the STAT3 site. Figure 1E reveals that this region was kept hypomethylated during the induction of spontaneous differentiation of neuroepithelial cells with 0.5% FBS. Taken together, these results suggest the existence of as yet unknown mechanisms, other than STAT3-site methylation, whereby neurons suppress a gene that is normally expressed in another lineage.

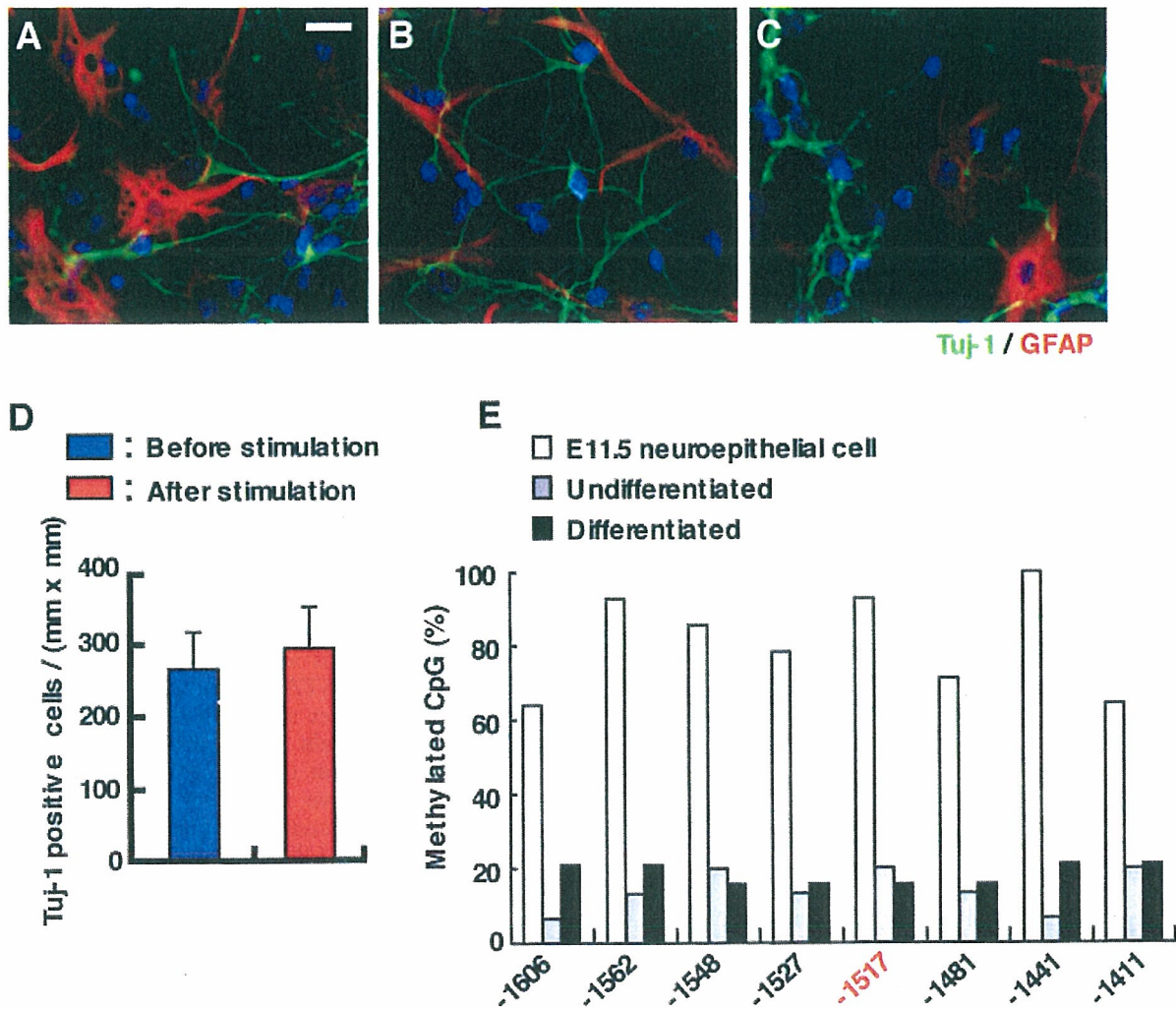


Fig. 1. Neurons generated from neuroepithelial cells at late gestation do not express GFAP even when stimulated by an astrocyte-inducing cytokine. **A:** Neuroepithelial cells were isolated from the telencephalon of E14.5 mouse brains, expanded in growth medium containing the mitogen bFGF, and differentiated in medium including 0.5% FBS. β III-tubulin-positive neurons (Tuj-1, green) and GFAP-positive astrocytes (GFAP, red) were identified with specific antibodies. Nuclei were stained with Hoechst 33258 (blue). **B,C:** After culture in the presence of FBS for 4 days, the medium was replaced by fresh growth medium but without bFGF. The cells were then cultured with (C) or without LIF (50 ng/ml; B) for an additional 4 days.

D: The numbers of Tuj-1-positive cells before and after LIF stimulation were counted (mean \pm SD). **E:** Methylation frequencies of the CpG site within the STAT3 recognition sequence (-1,517 bp, red) and of seven other CpG sites around this sequence in E11.5 neuroepithelial cells (white bars), undifferentiated E14.5 neuroepithelial cells (gray bars) and differentiated cells (hatched bars) were analyzed by bisulfite sequencing. The frequencies of clones having methylation at each CpG site are expressed as a percentage of the total number of clones sequenced (15–19 clones). Nucleotide position are designated base on GenBank accession number AY279974. Scale bar = 25 μ m.

MeCP2 Is Expressed Predominantly in Neurons

Given that GFAP was suppressed in neurons generated from neuroepithelial cells at late gestation, even when they were stimulated with LIF, we searched for transcriptional repressors expressed predominantly in neurons but not in astrocytes. It has been previously reported that MeCP2, MBD1, MBD2, and MBD3 are all expressed predominantly in neurons in the mammalian CNS (Coy et al., 1999; Jung et al., 2002; Shahbazian et al., 2002; Kishi and Macklis, 2004). Therefore,

we examined whether MeCP2, as a representative of the MBDs, is expressed specifically in neurons differentiated from E14.5 neuroepithelial cells under our culture conditions.

After 4 days' differentiation in 0.5% FBS-containing medium, the cells were stained with antibodies against MeCP2 and also against neuron and astrocyte marker proteins. As shown in Figure 2A, MeCP2 was expressed in neuronal marker (Tuj-1, Map2ab, and NeuN)-positive cells, but not in astrocyte marker (GFAP

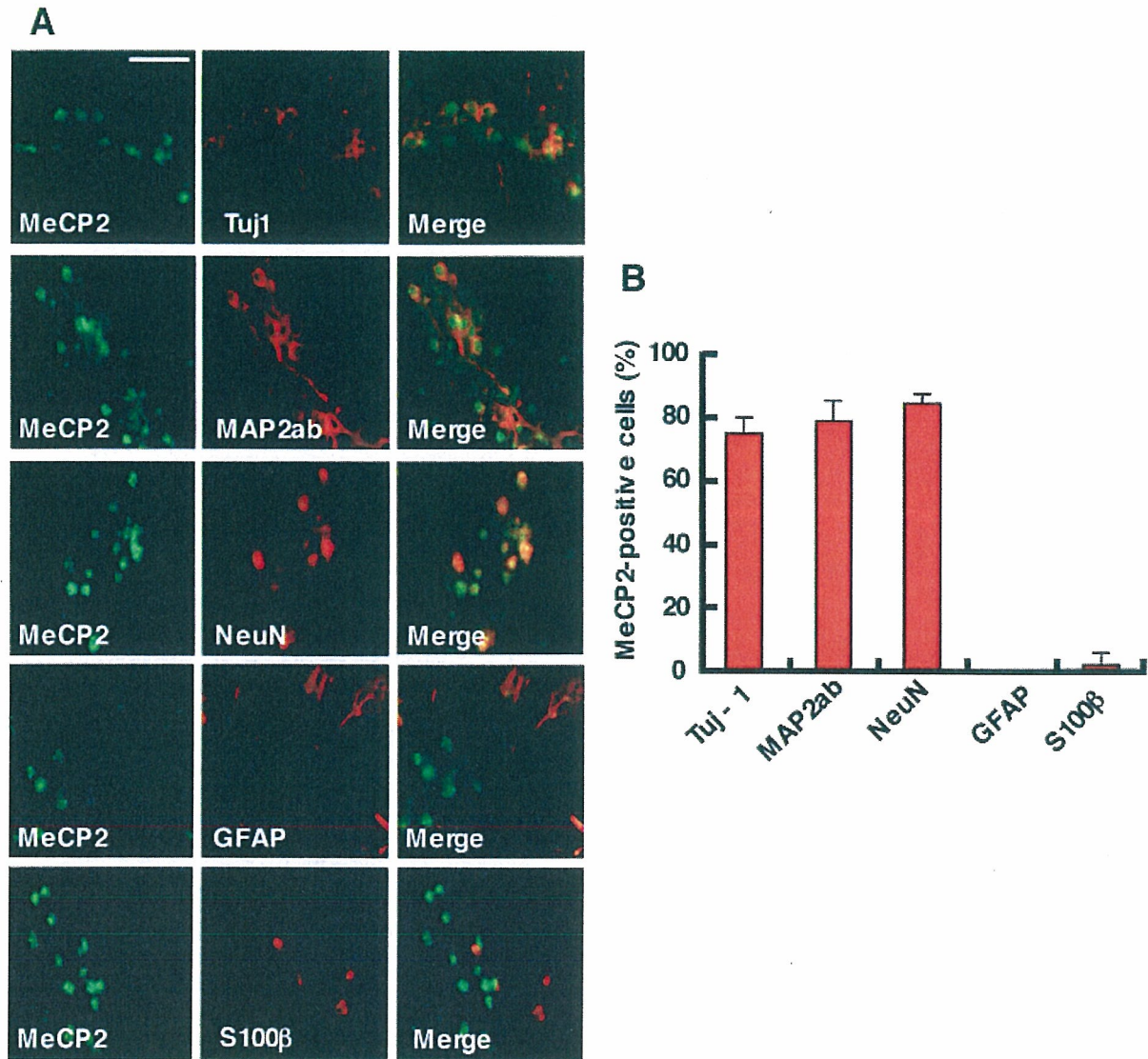


Fig. 2. Neurons but not astrocytes express MeCP2. **A:** Neuroepithelial cells were isolated from the telencephalon of E14.5 mouse brains, expanded in growth medium containing the mitogen bFGF, and differentiated in medium including 0.5% FBS. The cells were then stained with antibodies against MeCP2 (green), neuron markers

[βIII-tubulin (Tuj-1), Map2ab, or NeuN, red], and astrocyte markers (GFAP or S100β, red). **B:** The percentage of MeCP2-positive cells in each marker-positive cell population was quantitated (mean ± SD). Scale bar = 50 μm.

and S100β)-positive cells: 75%, 79%, and 84% of the cells positive for Tuj-1, MAP2ab, and NeuN, respectively, were also positive for MeCP2 (Fig. 2B). In contrast, very few cells, if any, were positive for MeCP2 among those expressing GFAP and S100β. These data indicate that MeCP2 is expressed predominantly in neurons but not in astrocytes.

Suppression of GFAP Expression by MeCP2

In light of the above-mentioned finding that the transcriptional repressor MeCP2 is expressed predomi-

nantly in neurons, we anticipated that MeCP2 would be able to suppress GFAP expression. To test this possibility, E14.5 neuroepithelial cells, which normally express GFAP in response to LIF, were infected with recombinant retroviruses engineered to express GFP (control) or both GFP and MeCP2. From the following day, the cells were continuously stimulated with LIF for 4 days to induce astrocyte differentiation. As shown in Figure 3A, the cells infected with control virus effectively differentiated into GFAP-positive astrocytes with LIF stimulation (54% in Fig. 3B). By contrast, MeCP2 expression in neuroepithelial cells dramatically inhibited the cells